Title: Hierarchical and dynamic seascapes: a quantitative framework for scaling pelagic biogeochemistry and ecology

Authors: Maria T. Kavanaugh[1, 2, 3], Burke Hales[2], Martin Saraceno [4,5], Yvette H. Spitz[2], Angelicque E. White[2] , Ricardo M. Letelier[2]

[1] Corresponding author, Department of Marine Chemistry and Geochemistry, Woods Hole Oceanographic Institution, Woods Hole, Massachusetts USA

E-mail address: (mkavanaugh@whoi.edu).

[2] College of Oceanic and Atmospheric Sciences, 104 COAS Administration Building, Oregon State University, Corvallis, Oregon, USA,

[3] Current Affiliation: Department of Marine Chemistry and Geochemistry, Woods Hole Oceanographic Institution, Woods Hole, Massachusetts USA

[4] Departamento de Ciencias de las Atmosfera y los Oceanos, Facultad de Ciencias Exactas y Naturales, Universidad de Buenos Aires, Argentina

[5] Centro de Investigaciones del Mar y la Atmósfera (CIMA/CONICET-UBA), UMI IFAECI/CNRS, Buenos Aires, Argentina

Acknowledgments:

We thank Curtiss Davis, Evelyn Sherr, Lisa Madsen, David Glover and Scott Doney for their intellectual contributions and assistance with geostatistical methods. The classification algorithm was substantially improved with help from Andrea Van Der Woude, Roberto Venegas and Russ Desiderio. This manuscript also benefited greatly from the comments of three anonymous reviewers. This project was partially funded by a NASA ESS fellowship NNX07A032H (MTK), an AAAS/ NPS scholarship (MTK), and funds from the NSF Science and Technology Center for Microbial Oceanography: Research and Education (C-MORE, RML and AW).

Keywords: North Pacific, seascapes, seasonal variations, pelagic environment, biogeochemistry, models

Highlights:

- Hierarchical, dynamic seascapes were classified using multivariate satellite data.
- Seascapes describe basin and gyre scale features and seasonal boundary shifts.
- Analyses of independent data reveal unique biogeochemical signatures among seascapes.
- Dynamic seascapes result in more efficient pattern classification than static provinces.
- Predicting $p\mathrm{CO_2}$ within seascapes reveals regional forcing and decreased model error.

Hierarchical and dynamic seascapes: a quantitative framework for scaling pelagic biogeochemistry and ecology

1. ABSTRACT

Comparative analyses of oceanic ecosystems require an objective framework to define coherent study regions and scale the patterns and processes observed within them. We applied the hierarchical patch mosaic paradigm of landscape ecology to the study of the seasonal variability of the North Pacific to facilitate comparative analysis between pelagic ecosystems and provide spatiotemporal context for Eulerian time-series studies. Using 13-year climatologies of sea surface temperature (SST), photosynthetically active radiation (PAR), and chlorophyll a (chl-a), we classified seascapes in environmental space that were monthly-resolved, dynamic and nested in space and time. To test the assumption that seascapes represent coherent regions with unique biogeochemical function and to determine the hierarchical scale that best characterized variance in biogeochemical parameters, independent data sets were analyzed across seascapes using analysis of variance (ANOVA), nested-ANOVA and multiple linear regression (MLR) analyses. We also compared the classification efficiency (as defined by the ANOVA F-statistic) of resultant dynamic seascapes to a commonly-used static classification system. Variance of nutrients and net primary productivity (NPP) were well characterized in the first two levels of hierarchy of eight seascapes nested within three superseascapes (R^2 = 0.5-0.7). Dynamic boundaries at this level resulted in a nearly 2-fold increase in classification efficiency over static boundaries. MLR analyses revealed differential forcing on pCO_2 across seascapes and hierarchical levels and a 33 % reduction in mean model error with increased partitioning (from 18.5 µatm to 12.0 µatm pCO_2). Importantly, the empirical influence of seasonality was minor across seascapes at all hierarchical levels, suggesting that seascape partitioning minimizes the effect of non-hydrographic variables. As part of the emerging field of pelagic seascape ecology,

this effort provides an improved means of monitoring and comparing oceanographic biophysical dynamics and an objective, quantitative basis by which to scale data from local experiments and observations to regional and global biogeochemical cycles.

2. INTRODUCTION

2.1. The necessity of a formal pelagic seascape concept

The pelagic ocean is a complex system in which organism distributions are affected by and provide feedbacks to physical and biogeochemical processes on multiple scales of spatial, temporal, and biological organization (Lubchenco and Petes, 2010, Doney et al., 2012). Non-linearities are common in biogeochemical (e.g. Gruber, 2011; Hales et al., 2012), biophysical (e.g. Hsieh et al., 2005) and trophic (Litzow and Ciannelli, 2007, Brander, 2010) interactions. Furthermore, spatial heterogeneity is ubiquitous and occurs at all scales observed (Steele, 1991; Levin and Whitfield, 1994; Mitchell et al, 2008). Understanding and modeling pelagic ecosystem responses and feedbacks to environmental perturbation is therefore hampered by the lack of an objective framework to (1) scale local processes to ocean basins (2) define how temporal and spatial scaling of habitats may change regionally, and (3) place the ‘snapshots’ of data collected in a typical oceanographic research expedition into a regional context.

To address issues of scale, change and context, terrestrial ecologists have looked toward the field of landscape ecology (Turner et al., 2001; Turner 2005). Terrestrial ecosystems are parsed into landscapes, defined in space by the main complex causal (Troll,1950) or reciprocal (Turner, 2005) relationships between the environment and the distributional patterns of organisms. Likewise, in the marine environment, physiological and ecological responses are closely coupled to the scale of physical forcing (Steele, 1989). Thus, the global ocean may be viewed as a mosaic of distinct seascapes, composed of unique combinations of physicochemical forcing and biological responses and/or feedbacks.

The characterization of distinct ocean ecosystems based on ocean color can be traced as far back as Somerville (1853); however, the most comprehensive approach combining geography, ocean color, and biogeochemistry can arguably be attributed to Longhurst (1998, 2007). The Longhurst classification used chlorophyll a (chl-a) from the Coastal Zone Color Scanner, ship-based climatologies of nutrients, euphotic depth and several physical variables describing water column stratification. Although the classified provinces are static, rectilinear, and subjectively chosen, the resultant framework has been instrumental in understanding changes in fishery and zooplankton distributions (Beaugrand et al., 2000) and optimizing biogeochemical models, particularly satellite primary productivity algorithms (Siegel et al., 2001). More recent efforts have used the maturing satellite data record to classify regions of biophysical coherence for coastal (Saraceno et al., 2006; Devred et al., 2007; Hales et al., 2012) and open ocean regions (Oliver and Irwin, 2008). The majority of these efforts have been temporally static (but see Devred et al., 2009 and Irwin and Oliver, 2009) and at a single scale. Importantly, few have verified their classifications with rigorous *post-hoc* statistical analyses using independent data sets at multiple scales (but see Vichi et al., 2011).

We classified satellite-derived seascapes in a spatially and temporally specific fashion and explicitly test the hypothesis that coherent regions as identified with satellite data represent distinct regions of ecosystem functioning (Platt and Sathyendranath, 1999). We extend the methods presented by Saraceno et al. (2006) and Hales et al. (2012) to resolve the intra-annual evolution of seascapes in the open North Pacific based on a 13-year climatology of satellite observations. Furthermore, we explicitly apply the concept of patch hierarchy (Kotliar and Wiens, 1990; O'Neill et al., 1992; Wu and Loucks, 1995). Borrowed from landscape ecology, the hierarchical patch mosaic paradigm views the system as a nested and partially ordered set, where system dynamics are defined by the composite of interacting, but distinct patches within the system. In our analysis, individual seascapes comprise the patches which aggregate (or split) to form superseascapes (subseascapes) at larger (finer) spatiotemporal scales. This application allowed us to classify basin-scale and gyre scale dynamics with the same domain and test hypotheses regarding resolution requirements for characterizing variability of different biogeochemical processes. First, we describe the general patterns of seasonal seascape variability across hierarchical levels. Then, we test the assumption that seascapes represent areas of distinct biogeochemical function by evaluating differences between seascapes using independent *in situ* distributions of nutrients, net primary productivity (NPP) and the partial pressure of carbon dioxide (pCO_2) in the surface ocean. On a subset of these data, we compare the efficiency of classification between seasonally dynamic seascapes and a commonly utilized static framework (Longhurst, 1998; 2007). Finally, we demonstrate the utility of the dynamic seascape framework in reducing model error and illuminating regional variability of biophysical forcing of important biogeochemical processes and patterns.

3. METHODS

3.1. Study Area

The North Pacific includes the oligotrophic and subarctic gyres that are separated by the broad North Pacific current, NPC (Figure 1). In the western basin, the strong Kuroshio (~3 km hr^{-1}) and Oyashio currents generate sharp physical and biochemical gradients. In the east, the NPC broadens and slows (~0.5 km hr^{-1}), bifurcating off the coast of British Columbia coast to form the Alaska and California Currents and contribute to the boundary circulation of the subarctic and subtropical gyres. The subarctic-subtropical transition zone from the Kuroshio extension into the eastern subarctic gyre is the largest sink region for atmospheric carbon dioxide in the North Pacific (Takahashi et al. 2009). Here, while biological uptake of dissolved inorganic carbon

(DIC) tends to counteract the warming effect in the summer, the bulk of the CO_2 drawdown coincides with winter cooling and the resultant increase in solubility of CO_2 in seawater (Takahashi et al., 2002).

Superimposed on the physical boundaries described above, seasonal and latitudinal changes in surface temperature (SST) and photosynthetically active radiation (PAR) contribute to defining the seascapes in which ecological assemblages develop and persist. In this study, we have selected to restrict the domain to 120-240º W, 15-65º N in order to highlight open ocean variability by minimizing the influence of extreme values associated with ice-edge responses in the northern latitudes and tropical instability waves that pulse along the equator in the southern portion of the North Pacific subtropical gyre (Evans et al., 2009).

3.2. Satellite data and processing

As a first step, we classified seascapes using remote sensing data that was related to phytoplankton dynamics, namely chl-a, PAR and SST. We used archived monthly averages and 8-day composites of the latest processing of satellite data provided by the Ocean Productivity Group (*www.science.oregonstate.edu/ocean.productivity*), as used in their primary productivity algorithms. These data have been cloud-filled which results in reduced variability at seascape boundaries that would otherwise have been associated with patchy cloud cover (Kavanaugh unpubl. data). We downloaded Level 3, 18 km binned, 8-day composites and monthly averages of SeaWiFS (R2010) chl-a, PAR, and Advanced Very High Radiometer sea surface temperature (AVHRR SST); the 18 km data were subsequently binned into ¼ degree pixels. The SeaWiFs (SW) data record extends from 1998-2010 albeit with episodic gaps during 2008-2010 due to sensor failure. Where missing, SW chl-a and PAR were interpolated using the comparable MODIS (R2012) product. Linear regression was conducted at each pixel using the eight-day composite of each sensor for each month over the years 2003-2010. Predicted SW chl-a did not vary more than 25% from actual SW chl-a (usually less than 10%) and predicted PAR varied less than 10% from actual SW PAR. The predicted 8-day composite was then used to fill gaps in the real SeaWiFs 8-day composites; monthly averages were computed from the combined product. Chl-a values >8 mg m^{-3} were masked to minimize the effect of coastal variability and maximize variability in the open ocean. The chl-a field was $\log_{10}$-transformed. All three fields were normalized (to a scale of -1 to1) prior to classification, where the maximum value would be 1, minimum -1 and median=0.

3.3. Hierarchical classification of dynamic seascapes

Because of the strong, complex coupling of phytoplankton to physical forcing at cellular (Jassby and Platt, 1976), local/community (Steele and Henderson, 1992; Belgrano et al., 2004) and mesoscales, we chose a classifier that was robust to nonlinear interactions, maintained underlying biophysical distributions, and allowed seascapes to be defined objectively at multiple, nested scales. In brief, we used a probabilistic self-organizing map (PrSOM, Anouar et al., 1998) combined with a hierarchical agglomerative classification (HAC, Jain et al., 1987) to achieve a non-linear, topology-preserving data reduction. SOMs have been used in oceanography to classify regions (e.g. Richardson et al., 2003; Saraceno et al., 2006), define regions of mechanistic coherence in predictive pCO_2 models (Hales et al., 2012), and to find drivers of net primary productivity (Lachkar and Gruber, 2012). As with most SOM methods, PrSOM uses a deformable neuronal net to maintain data similarities and topological order between clusters. However, the PrSOM introduces a probabilistic formalism: clusters are produced by approximating the probability density function with a mixture of normal distributions and optimization based on a maximum likelihood function (Anouar et al., 1998).

The PrSOM algorithm and PrSOM-HAC combination algorithm are described in detail in Anouar et al. (1998) and Saraceno et al. (2006), respectively. We follow the method of Saraceno et al. with two exceptions: (1) monthly climatological grids were vectorized and concatenated to allow classification of space and time simultaneously, and (2) we chose multiple objective function thresholds (below) to allow for multiple hierarchical levels to emerge. Briefly, PrSOM reduces the spatiotemporal D-variable pixel vectors data set sequentially onto a M×N neuron map. In our case, D=3 : SST_{xyt}, PAR_{xyt}, chl-a_{xyt}, where x,y, t denote the particular geographic coordinate and month of the pixel vector. Pixel vectors remain or move amongst neurons in an iterative fashion that optimizes a fit to a D-variate Gaussian distribution and maximum likelihood estimates (MLE) for each variable are calculated. As in simulated annealing, the trading distance expands and contracts (Anouar et al., 1998), with a maximum distance in our case set to three (~20% of total topological distance) and maximum iterations set to 1000. The neural map size (M x N=225) was chosen to maximize sensitivity to mesoscale processes while preventing underpopulated nodes (defined as less than 500 pixels). The map shape (M=N, square) was chosen for its simple geometry to minimize topological edge effects. The result after the final iteration were 225 weight vectors, each weight a MLE of a particular variable for a given neuron.

The 225 weight vectors were reduced further by using a hierarchical agglomerative clustering (HAC) with Ward linkages (Ward, 1963). This linkage method uses combinatorial, Euclidian distances that conserve the original data space with sequential linkages (McCune et al., 2002). With each agglomeration and formation of a new seascape cluster, distances are recalculated to determine the distance of each vector to both its cluster centroid and the global centroid, equivalent to within-group and total sum of squares (GSS and TSS, respectively).

An objective function (I, information remaining; McCune et al., 2002) was determined a priori to define the total number of seascapes:

1. $I = (TSS-GSS)/TSS$

where TSS=GSS when all seascapes are fused into one. To define seascapes at emergent scales by which we would evaluate the differences in biogeochemistry, we examined stepwise agglomerations of seascape classes (C), which resulted in local, rapid shifts in I. We compared the shift in the objective function of our actual data (D) to that which would occur under a random spatial structure (R) where increased class size would add (1/C) information. We then determined whether the proportional shift was greater (aggregated) or less (dispersed) than unity by defining an aggregation index (AI):

2. $AI = 1-[(I_C(D) - I_{C-1}(D)) / (I_C(R) - I_{C-1}(R))]$.

3.4 Internal Validation of satellite-derived seascapes

3.4.1 Post-hoc statistical verification. To conduct parametric post-hoc summaries, we accounted for autocorrelation and anisotropy in our remote sensing dataset and resampled at data densities that were statistically independent. Autocorrelation, ρ, and number of pixel pairs, Np, at a given distance (d) and azimuth (a) were calculated with the original $\log_{10}$-transformed chl-a data for each seascape as a function of 10 km binned distance and 45-degree binned direction. A local correction factor ($\theta_{(d, a)}$) for each distance-azimuth bin was calculated according to Fortin and Dale (2005) where:

3. $$\theta_{(d,\,a)} = (1-\rho_{(d,\,a)}) / (1+\rho_{(d,\,a)})$$

A global correction factor, θ_{G}, was calculated for each seascape using a weighted average of $\theta_{(d,\,a)}$ using the weights $Np_{(d,a)}$:

4. $$\theta_G = \sum_{a=1}^{4} \sum_{d=10}^{d_{max}} [\theta_{a,d} N p_{a,d}] / \sum_{a=1}^{4} \sum_{d=10}^{d_{max}} N p_{a,d}$$

where d_{max} was the lesser of 600 km or 0.6 x distance to seascape edge. The global correction factor ranged from ~0.15 to ~0.4 (see Table 1) and was applied to the total number of pixels in a sample, *N*, to obtain the effective sample size, *N'* for each seascape x month interaction:

5. $$N' = \theta_G N$$

Subsequently, *N'* multivariate pixels were randomly selected for statistical comparison to test whether provinces result in different multivariate means. *N'* was calculated for each month x seascape; all three fields were randomly resampled at the *N'* level. Because data tended to be positively correlated at local and mesoscales and anticorrelated at larger scales, this limit resulted in a smaller effective sample size and therefore a more conservative estimate of seascape differences.

3.4.2 Sensitivity. Classification algorithms that use different sensors, attributes, assumptions of linearity, or dispersed organizational structure will result in different division of state space and thus, the spatiotemporal location of seascapes and their boundaries. Here we focus on how robust post-hoc boundaries are to interannual changes in chl-a, via changes in community structure or unmeasured physical forcing such as mixed layer depth or eddy kinetic energy. Seascapes were classified as in Section 3.3 for each year, using the climatological means for SST and PAR, and the individual years' monthly means for chl-a. Area of pixels were calculated (27.5 km x cosine (latitude) x 27.5 km for ¼-degree resolution) and total areal coverage summed for each seascape. Seasonal patterns of expansion and contraction for individual years were compared to the climatological pattern for each seascape. Interannual shifts in boundaries associated with large-scale shifts in physical forcing are the focus of a different manuscript.

3.5 External validation of satellite-derived seascapes

3.5.1 Evaluation of biogeochemical differences among seascapes

Differences in biogeochemical factors and processes among seascapes and the relative importance of seascapes compared to space and time were determined by evaluating archived nutrient concentrations, net primary productivity (NPP) and pCO_2 data. Surface concentrations of nitrate (NO_3^-), phosphate (PO_4^{3-}) and silicate (SiO_{2aq}) were downloaded from open ocean stations (N >12000) archived in the World Ocean Database, WOD (v.2009; http:// www.nodc.noaa.gov); data were subsequently binned into the nearest 1x1 degree pixel and monthly means were calculated (final N=3985). Climatological net primary productivity, NPP, was determined using monthly climatologies (1998-2010) of the updated carbon-based primary production model (Westberry et al., 2008) made available by the Ocean Productivity group (http://www.science.oregonstate.edu/ocean.productivity/). Monthly climatological data of the partial pressure of CO_2 in surface waters (pCO_2) were downloaded from the Lamont-Doherty

Earth Observatory database (http://cdiac.ornl.gov/oceans/), and evaluated at the density reported by Takahashi et al., 2009.

3.5.2 Comparison to Longhurst provinces

The North Pacific is represented by nine Longhurst regions that are seasonally static: Bering Sea (BERS), Subarctic East (PSAE), Subarctic West (PSAW), Kuroshio (KURO), Polar Front (NPPF), Subtropical West (NPSW), Subtropical Gyre (NPSG), and the Alaska (ALSK) and California Current Systems (CCAL) (Longhurst, 1998, 2006). Polygons delineating these regions were downloaded (http://www.vliz.be) and gridded to a 0.25-degree surface. The Alaska Current province did not have sufficient data density within the uninterpolated WOD set; thus, comparisons to emergent seascapes were made among the remaining eight provinces.

3.6. Statistical Analysis

All statistics were performed using JMP v 8.2 (© SAS Institute, Cary NC). Satellite-derived seascape, nutrient and pCO_2 data were grouped according to seascapes and month. Summary statistics are reported for *in situ* data and for satellite data (post decorrelation) from analysis of variance (ANOVA) with Tukey-Kramer adjustments for multiple comparisons and different sample sizes. Nested ANOVA (nANOVA) were conducted to determine the relative importance of different hierarchical levels, or seasonality and space within a single hierarchical level on nutrients, nutrient ratios, and pCO_2. Rather than arbitrarily assign season bins across a wide latitudinal extent, season was modeled by fitting a sine function to month of year (season=sine (month/4)), which resulted in a simplified seasonal cycle approximating the patterns of solar irradiance. Spatial variability was modeled as a function of the interaction of latitude and longitude, with the longitude function representing degrees from the dateline. These variables were included as a metric to gauge the relative importance of continuous variability within seascapes.

To assess the relative importance of different biophysical interactions across seascapes, a multiple linear regression model was built to determine the effect of SST, chl-a, salinity and season on pCO_2 within seascapes. All regression coefficients were scaled by their dynamic ranges and centered on their means to produce a standardized effect size. Individual effect sizes are thus unit-less and can be interpreted the percent change in pCO_2 that is associated with a percent change in the driver after accounting for weighted effects of other significant drivers. Effect sizes (+/- standard error) were compared between parameters and across seascapes and scales.

We compared the dynamic, objectively defined seascapes described above to the static, subjectively defined seascapes described by Longhurst based on their relative efficiency in partitioning variance of representative biogeochemical variables. The choice of variables reflects an attempt to remain neutral for intercomparison while using available synoptic data: chl-a was used explicitly in both the PrSOM-HAC and Longhurst classification, nutrients were explicit in Longhurst classification and variability in NPP may be considered implicit in both schemes. Common summary statistics from post-hoc ANOVA to verify classification schemes are the F-statistic, a ratio of between-class variance to within-class variance, and the R^2, a measure of total variance explained. Because the latter can be biased to total number of classes, we compared the F-statistic (F-stat) between classification schemes. To account for different spatial sampling, NPP and chl-a were resampled at the location of the WOD nutrient casts. Classification efficiencies within the year and across variables were compared using pair-wise t-tests.

4. RESULTS

The PrSOM-HAC combination resulted in optimized clusters that accounted for approximately 90% of variance in climatological means of satellite-derived chl-a, SST, and PAR (Table 1). There were three distinct local maxima in the objective function (Figure 2a) from which we derived three levels of nestedness (Figure 2b). While month-wise spatial decorrelation resulted in a reduction of ~80% of the data, seascapes were still significantly different for all variables considered and at all scales ($p<0.05$ Tukey-Kramer HSD test), with the exception of chl-a between two clusters at the finest resolution (Table 1). In relative terms, increased resolution to eight seascapes resulted in small, but significant, addition of variance explained for chl-a and SST, but a larger increase in variance of PAR explained. Thus nesting eight seascapes within three superseascapes resulted in the characterization of the seasonal cycle of insolation, warming and biological response for the North Pacific (Figure 2c). Seascape mean states and the boundaries that define them should be interpreted as the combination of advection and local shifts in chl-a, SST, and PAR. Spatiotemporal patterns are described in detail below.

4.1. Spatiotemporal hierarchical patterns

4.1.1. First-level dynamics

At the basin scale, three distinct seascapes were classified that generally describe the known divisions between the subarctic, transition and subtropical regions (Figures 2b, 3). All three areas are present year round, with the transition zone approximating the division between the transition zone chlorophyll front (TZCF, Polovina et al., 2001) and the subarctic front. The Kuroshio extension was evident in February and the eastern north Pacific bifurcation became evident in

May. Most of the seasonal dynamics, however, were limited to latitudinal variation in the location of the transition zone.

4.1.2. Second-level dynamics

At the second level of hierarchy, eight total seascapes were classified (Figure 2b, Figure 4) that generally described basin scale seasonality. Three seascapes each arose from the subtropics and subarctic whereas two seascapes resulted from division of the transition zone. Note that the number of seascapes found in each month was different and that a given seascape usually occupied a shifted geographical region as the time of year varied. Since the methodology distributed the seascapes in space and time in order to minimize the within-seascape variance of the variables considered, it was possible to follow the same composite properties by following a given seascape in time. Seascapes were nominally identified based on dominant season, geographic region and/or trophic status based on mean chl-a concentration, specifically: 1) Summer subtropical (Su-ST); 2) Winter subtropical (W-ST); 3) Oligotrophic boundary (OB); 4) Winter transition (W-TR); 5) Summer transition (Su-TR); 6) Mesotrophic boundary (MB); 7) Winter subarctic (W-SA); 8) Summer subarctic (Su-SA).

In January, latitudinal variations in light separated the four winter seascapes: W-SA, MB, W-TR, and W-ST, with only minimal expression of Su-TR present in the extreme southeast part of the study region (Figure 4). February marked the expression of the Kuroshio extension with high chl-a in seascape W-TR and differentiation of regions abutting the North Pacific current. Concurrently, the OB seascape expanded eastward, bifurcating W-ST into northern and southern components. In March, high chl-a water from the Oyashio current and the Sea of Japan was entrained in the subarctic front, illustrated by the cross-basin expansion of the Su-SA and MB seascapes, while W-TR and W-ST disappeared. April marked the onset of a spring transition with abrupt shifts in seascape identity: The W-SA seascape, which persisted Jan-Mar, disappeared entirely and was replaced by Su-SA. May, June, and July were similar to April, distinguished primarily by the northeastward expansion of Su-ST and the N-S broadening of MB north and south along the North American continent. During this time, the interface between the two boundary seascapes tended to follow the seasonal migration of the TZCF. During August, the Su-SA zone was replaced by the MB seascape, while the Su-TR zone became constricted by the expansion of MB from the north and the OB from the south. September was similar to August, although the fall transition began then with the first hints of the W-ST encroaching from the southwest and the W-SA in patches within the Alaska Gyre and in the SW along the boundary of the Oyashio and Kuroshio. The fall transition was most clearly expressed in October, with the Tr-SA zone retreating from the open SA towards the continents, the first break in the cross-basin expanse of MB since February, and the first widespread appearance of the three winter zones.

The progression of seascapes found in our analysis gives a new perspective on seasonality in the North Pacific. On a basin scale, winter appears to consist of three months spanning November – January, and was defined by the full cross-basin expression of W-ST and W-SA seascapes. Summer, defined by the cross-basin extent of the Su-TR and OB zones, accompanied by the expansion of Su-ST to the south and Su-SA persists for five months (April – August). Fall, defined by the first absence of defined summer or boundary zones, and first appearance of winter zones, was most clearly expressed in October, although hints of transition are evident in September at higher latitudes. The spring transition, defined by the first cross-basin appearance of the boundary seascapes and the first appearance of the Su-ST and Su-SA zones, was most clearly defined in March, although changes from winter conditions were evident in February.

4.1.3. Third level dynamics

Fourteen seascapes emerged at the finest hierarchical level. These seascapes were nominally identified by their relative [chl-a] and were indexed SS1 to SS14 (Figure 2b, Figure 5). Increasing hierarchical resolution from eight to fourteen seascapes did not affect the boundaries of the two subtropical seascapes (Su- and W-ST= SS1 and SS2 respectively), however, it split each of the remaining six seascapes.

In general, the resultant seascapes represented increased spatial variability in the subtropics and seasonal opposites at higher latitudes. The OB split into two distinct subseascapes, SS3 and SS4, both present for all but two months of the OB duration (March-September vs. February- October). The W-TR split into two distinct subseascapes (SS5 and SS6) marked primarily by latitudinal differences in temperature and light. The Su-TR split into two seascapes (SS7 and SS9) that seasonally represented marginal ecosystems (e.g. the California Current). From the sixth seascape (MB), distinctions arose associated with the spring (SS8) and fall (SS12) transition in the subarctic with seascapes that identify the Kuroshio extension in February and April and the California current in early spring and late autumn. The seventh seascape (W-SA) split (SS10 and SS11) to include a higher chl-a region (SS11) apparent in the subarctic in October that shrank to align with the boundary regions in the winter. Finally, the division of the Su-SA seascapes allowed for the slightly different spatiotemporal dynamics of the eastern (SS 13) and western subarctic gyres (SS14).

4.2. Sensitivity

In general, the classification was robust to local shifts in chl-a as (Figure 6). For most seascapes and months, local shifts in [chl-a] resulted in < 5 % change in seascape extent. The exception occurred in the subtropical summer. Here shifts in chl-a were associated with decreased classification rates to the Su-ST which manifested in decreased summer expansion in the Su-ST and increased summer expansion in the OB relative to the climatology. This suggests that classified boundary between these two systems is relatively diffuse. Nevertheless, the timing of expansion and contraction remained as robust in the subtropics as in the transition and subarctic seascapes.

4.3 In situ data evaluation

4.3.1 Biogeochemical patterns

Here we tested the hypothesis that seascapes represent a framework for describing biogeochemical distributions. Indeed, seascapes explain a significant portion of variance of nutrient concentrations. Because nesting was unbalanced (Su-ST and W-ST in two hierarchical levels), absolute effects could not be translated into percent of model explained. However, the relative effect of nesting levels was determined by examining the F-statistics (Table 2). In most cases, the greatest amount of variance was explained by the coarsest level of hierarchy, although nested levels still explained significant variation (Table 2). The exception to the dominance of Level 1 occurred with NPP, where Level 2 (characterizing the seasonal cycle) resulted in the largest contribution of variance explained in the fully nested model (Table 2: F-stat= 312) and $p\mathrm{CO_2}$ where higher resolution resulted in better characterization of variance (F-stat of Level 3 > Level 1> Level 2). For salinity and nutrients, nesting continuous temporal and spatial variability within seascapes results in minimal increases of explanatory power (Table 3) after accounting for differences among seascapes. However, the effect of seasonality was strong for NPP, suggesting that subseascape temporal shifts contribute significantly to total variability (Table 3: seascape F-stat= 17.6; season F-stat = 79.1). The role of space and time within seascapes was also somewhat strong for pCO_2, but contributed less than that of differences among seascapes (Table 3: seascape F-stat=15; season= 10; space= 5).

Biogeochemical patterns tended to coincide with basin scale variation in temperature and salinity, with the lowest nutrient concentrations and in Su-ST and highest nutrient concentration in the Su-SA. However, other variables did not follow this pattern. Within the subtropics, nitrate was not different between seascapes but PO_4, and to a lesser degree SiO_2, increased from Su-ST to OB (Table 4 and Level 2 Tukey-Kramer HSD test: Su-ST<W-ST<OB, p<0.05). This led to low N: Si and N: P in the OB compared to other subtropical seascapes and its northern neighbor (Table 4 and Level 2 Tukey-Kramer HSD test: OB< W-ST~Su-ST<W-TR, p<0.05). pCO_2 also had a local minimum in the transition zone (Table4 and Level 1 Tukey-Kramer HSD test: Transition < Subarctic < Subtropics, p<0.05). Finally, while rates of satellite-derived NPP were highest in the Su-SA, (Table 4, mean NPP=660 mg C m-2 d-1), NPP was <10 % lower in the Su-TR (mean NPP=600 mg C m-2 d-1) and significantly higher than in the remaining seascapes (Level 2 Tukey-Kramer HSD test, p<0.05).

4.3.2. Dynamic seascape and Longhurst comparison

The F-statistics (Table 5) are a measure of the ratio of the average between-group variance to the variance within a group, and thus a general means by which to compare the efficiency of variance partitioning of different classification schemes. We examined the efficiency of the different classification schemes for capturing the spatial variability throughout the year of: chl-a (included explicitly in the PrSOM-HAC classification), surface PO_4 (included in explicitly in the

Longhurst classes) and NPP (included in neither but implied by both through choice of classifying parameters). Within individual months and across the annual cycle, PrSOM-HAC-based classification was more efficient at capturing variability in chl-a. The differences between classification schemes were minimal in winter and maximal in early summer, with the efficiency of PrSOM-HAC seascapes being more than 2.25X greater than that of Longhurst provinces for classifying chl-a variability over the annual cycle. Within months, with the exception of February through April, PrSOM-HAC derived seascapes explained more variability of NPP than did the Longhurst provinces (Table 5); on average, the efficiency of the PrSOM-HAC classification was 65% higher than of Longhurst (F-stat=53.7 compared to F-stat=32.0). For PO_4 within months, PrSOM-HAC derived seascapes resulted in greater between-group variability than Longhurst provinces for most months considered, with increased classification efficiency of > 50% on average over the year. The PrSOM-HAC approach is therefore a better predictor of conditions even when examining parameters not explicitly included in PrSOM-HAC that were explicitly included by Longhurst.

4.4 Biophysical forcing of pCO_2

The biophysical forcing on pCO_2 varied as a function of seascape and hierarchical level (Table 6, Figure 7). In preliminary analyses, chl-a was found to be a stronger predictor of pCO_2 than was NPP when both were included in the model; the latter was therefore not included in subsequent analyses. With the exception of one seascape in the second level, seasonality was a relatively minor effect on pCO_2 across all hierarchical levels. Furthermore, substantial variation in North Pacific pCO_2 was explained by constraining of the dynamic range of explanatory variables of the simple MLR model within seascape spatiotemporal boundaries (Table 5). The multiple linear regression analysis explained up to 88% and typically >60% of the variability. Correlations (after accounting for sample density within each seascape) averaged 0.68 for the coarsest level, 0.73 for level 2 and 0.70 for level 3. Root mean square error of the multiple linear regression model was also reduced with finer resolution. Across seascapes, pixel weighted mean RMSE (+/- SE) decreased from 18.5 µatm (basin) to 15.3 (+/-1.6) µatm at Level 1 to 12.4 (+/-1.1) µatm at Level 2 to 12 (+/-0.8) µtam at Level 3.

In the subtropics, at the coarsest scale, $p\mathrm{CO_2}$ decreased as a function of increased chl-a, cooling, and wintertime processes not related to cooling. $p\mathrm{CO_2}$ also increased with decreased salinity in this region. With increased resolution (Level 2), the negative salinity effect appeared to be driven by dynamics in OB with positive associations of salinity in both Su-ST and W-ST. The OB was unique also due to the strong contribution of chl-a to $p\mathrm{CO_2}$ drawdown.

Across the transition zone, chl-a had the strongest effect on $p\mathrm{CO_2}$ (Table 5, Figure 7). SST was not a significant factor in this region when changes in salinity were included. The chl-a effect was significantly greater than warming effect in this region for the first two levels of hierarchy, however, the relative effects in the third level could not be resolved in many regions due to decreased sample size.

In the subarctic, physical mixing appeared to be the dominant factor in driving $p\mathrm{CO_2}$ in our model, with strong positive salinity effects, both in W-SA and Su-SA. While chl-a was a significant driver of $p\mathrm{CO_2}$ in the subarctic in general, its effect was dwarfed by the mixing signal of salinity and cooling signal of SST in all but the MB seascape.

5. DISCUSSION

Because of the challenges inherent to working in an advective environment and with organisms that exhibit patchy distributions on multiple scales, seascape ecology requires a sound framework for analyzing spatiotemporal patterns in the structure of pelagic assemblages and the biogeochemical function they provide (Karl and Letelier, 2009). The utility of the seascape framework described here is supported by three lines of evidence: 1) hierarchically organized seascapes generally follow known patterns of circulation and characterize the seasonality of the North Pacific, allowing for objective extrapolation of observations in space and time; 2) seascapes represent unique spatiotemporal entities, describing distinct surface nutrient and primary productivity regimes; 3) seascapes represent distinct biophysical interactions that are relevant to predicting important processes such as regional variability in the biophysical forcing of pCO_2. Furthermore, the framework that we present improves upon the static approach of Longhurst and allows for objective scaling of phenomena in space and time.

5.1 Hierarchical organization and scaling. The North Pacific has several seasonally distinct features that exhibit a spatiotemporal hierarchy. Our seascape classification allowed visualization of the onset of the Kuroshio extension, the Oyashio bloom and entrainment into the subarctic frontal current, and the seasonal and meridional changes in the transition region between the oligotrophic subtropical and the productive subarctic gyres (Figure 2-4). The dynamics of these transition zones were also apparent with higher order clustering, as were heightened seasonality in the subarctic and transition regions (Figures 3 and 4). Importantly, our classification allowed for non-linear interaction between attributes and allowed for hierarchical organization and seasonal expansion of seascapes that were robust to local variability of a single variable, e.g. chl-a.

As suggested by previous studies (Devred et al., 2008; Hales et al., 2012), we clearly show that seasonally evolving boundaries characterize the dynamics of marine systems better than static, rectilinear boundaries. However, classification error or uncertainty increases when the gradients are subtle and or the variability within each seascape is high relative to the mean. In the subtropics, where SST and PAR are co-linear and the chl-a signal is low and relatively stable, the classification was sensitive to local changes in chl-a in the subtropics, resulting in over-estimation of the mid-summer Su-ST extent and underestimation of the OB extent . The boundary uncertainty is also reflected in the similar chl-a values for the climatological means of the Su-ST and the OB, which suggests that shifts in PAR and SST, rather than "biology" may drive this seascape division. However, in a given year, late summer eddies that regularly occur along 30 °N (Wilson et al., 2008) may drive the ST-OB boundary further south, whereas the climatological signal may be dampened by spatial variability between years. In addition, chl-a seasonality in the Su-ST at Station ALOHA (Letelier et al. 1993, Winn et al., 1995) and at the Su-ST: OB boundary region (Siegel et al., 2013) is known to be dominated by mixed layer dynamics and changes associated with photoacclimation rather than shifts in phytoplankton abundance. Thus, there remains uncertainty to the nature of the Su-ST division and how it is affected by local variation in physical forcing, acclimation and shifts in phytoplankton abundance and community structure. However, despite the uncertainty, the different nutrient ratios and biophysical forcing of $p\mathrm{CO}_2$ suggest that the two seascapes function differently. Certainly, future efforts should take advantage of improved synoptic mixed layer depth models and or satellite-derived salinity. These efforts will likely reveal greater complexity in the seascape mosaic, even at the seasonal scale, and should be validated with biogeochemical and ecological data sets.

5.2. Distinct biogeochemical distributions. The seasonal cycle of nutrients, nutrient ratios, and NPP in the North Pacific is described by the boundaries of satellite-derived seascapes suggesting that seascapes demarcate natural boundaries in nutrient availability and or nutrient use. Differences between seascapes accounted for a large amount of variance in both nutrient concentrations and nutrient ratios; seascape differences were also more important than both spatial and temporal variation within seascapes. While nutrient concentrations across seascapes followed patterns expected from satellite chl a data, distinct minima in surface N:P and N:Si occurred within the oligotrophic boundary seascape. This region is well documented to have persistent, albeit modest rates of N_2-fixation overlain by irregular summer-fall blooms of diazotrophs (Karl et al., 2012; Wilson et al., 2008; White et al., 2007) with N_2-fixation affecting subsurface nutrient distributions from the TZCF into the subtropics (Deutsch et al., 2001). Accordingly, tracking the spatial and temporal migration of the OB may be analogous to tracking the optimal habitat in the surface ocean for specific diazotrophs that would be selectively favored in low N: P or N: Si environments, particularly diazotrophic symbionts in diatoms (Venrick, 1974; Villareal, 1991). Certainly, iron deposition (Dutkiewicz et al., 2012), irradiance, or nitrate loss through denitrification upstream (Luo et al., 2013) may play a role in biogeographic patterns of diazotrophs, although the *in situ* verification of iron availability as well as diazotroph abundance has been has been historically limited (but see Luo et al., 2012).

Surface biogeochemical distributions appear to have a seasonally evolving biogeographic signature, although circulation and biological effects on these distributions could not be resolved.

Whether this dynamic, biogeochemical geography is associated with shifts in phytoplankton distributions (e.g. Weber and Deutsch, 2010) remains to be seen through careful experiments that manipulate biogeochemical and ecological models. We did not explicitly include phytoplankton assemblage information in our study, nor have we yet addressed interannual variation in seascape boundaries. Linking the seasonal and interannual dynamics of seascapes and their shifting boundaries to shifts in phytoplankton diversity and biogeochemical pattern remains a logical next step.

5.3. Unique biophysical interactions. One of the major goals of a dynamic seascape framework is to illuminate regional patterns and drivers of biogeochemical processes to improve understanding of underlying mechanisms and better parameterize global models. Regional variability is evident in the discrete comparison of PrSOM-HAC based and Longhurst-based partitioning. PrSOM-HAC based partitioning was more efficient in explaining seasonal and spatial variability of chl-a, PO_4 and satellite-derived NPP than Longhurst-based provinces. We recognize that these response variables are inter-related (e.g. the satellite-derived carbon based NPP uses the nitricline depth to establish C:chl-a ratios, Westberry et al., 2008); continued cross comparison using available independent datasets particularly with taxon- or rate- specific *in situ* or modeled measurements will be ultimately necessary. Nevertheless, we show that PrSOM-HAC based partitioning is more efficient at classifying seasonal biogeochemical variability, even of data used to inform Longhurst classification- both explicitly (nutrient) and implicitly (NPP). This general finding is supported by other observations (Hardman-Mountford et al., 2008) or statistical comparisons (Vichi et al., 2011): a single Longhurst province cannot account for the seasonal environmental variability in many regions of the ocean. Furthermore, constructing models within PrSOM-HAC based seascapes does not rely on a large seasonal parameterization (Hales et al., 2012). Changes in model performance and parameterization across seascapes can be interpreted as likely dependence on measured hydrographic parameters, rather than some unknown seasonally varying process. Dynamic objective seascapes may serve, therefore, as a more accurate extent than static frameworks by which to intercompare models and improve their parameterization.

Several investigators have recognized the challenges of predicting pCO_2 based on its highly variable dependence on different biophysical parameters in space and time. Park et al. (2010) used empirical subannual relationships between climatological pCO_2 and sea surface temperature, along with interannual changes in SST and wind speed to predict changes in surface pCO_2. Permitting the subseasonal regressions to be fit on any three or more sequential months allowed for different phases and shapes of the annual cycle and reduced the error for the pCO_2: SST relationship for a given coordinate. In the North Atlantic, using a similar domain size to ours, Friedrich and Oschlies (2009) trained a SOM-based predictive model with ARGO data by explicitly including latitude, longitude, and time in the training set. Telszewski et al. (2009) predicted pCO_2 by associating pCO_2 with a SOM-based classification of mixed layer depth, SST, and chl-a. While this method did not rely on bioregionalization, the predictive capacity in space and time was limited by the location and timing of the training pCO_2 data set. Hales et al. (2012) found that regional prediction of pCO_2 within static, but objectively-classified coastal seascapes was markedly improved by including time-dependence in a semi-mechanistic model. As suggested by Hales et al. (2012), the implicit inclusion of time in the classification of state space allowed us to diminish the effect of time in our simple predictive pCO_2 models. While satellite-based estimates may suffer from large gaps (Friedrich and Oschlies, 2009), we found that classification of coherent biophysical regions- i.e. seascapes, using only a subset of the available satellite record, resulted reduced hydrographical variability within a given seascape and increased model prediction capacity. Furthermore, while the classification inputs and statistical model inputs were similar, they were, with the exception of chl-a, from independent sources. Thus, seascapes may provide a means by which to test different hypotheses regarding the relative importance of different biophysical forcing and to conduct comparisons of oceanic ecosystem functioning (Murawski et al., 2010).

Seascapes represented regions of distinct biophysical forcing of $p\mathrm{CO_2}$. We were able to describe a transition zone divided into several regions within which biological and physical factors interact differently to modulate $p\mathrm{CO_2}$ and, potentially, air-sea $\mathrm{CO_2}$ flux. Considering processes within these distinct seascapes may help elucidate differential controls of the complex ecological phenomena such as how the biological pump contributes to air-sea exchange. For example, abutting the transition zone to the south, the oligotrophic boundary seascape may respond with diazotrophy-fueled blooms to draw down surface $p\mathrm{CO_2}$. In the northernmost seascapes, the drawdown effects of $p\mathrm{CO_2}$ by both cooling (via SST) and net community productivity (via chl-a) seemed to be small relative to mixing. In the transition seascapes, where spring-summer NPP was greater than any other seascape, the chlorophyll effect on $p\mathrm{CO_2}$ was greater than the temperature effect, whether coarsely or finely defined in the hierarchy. We note that coefficients were similar across the MB, OB, and the two transition seascapes, albeit with dampened seasonality effects and less predictive error in the transition seascapes. This similarity may be a result of over partitioning but it is also likely that our simple predictive model underestimates spatial variability by omitting processes such as mesoscale circulation and wind.

While we acknowledge that interannual variability may play a role in boundary location along the transition zone (e.g. Bograd et al., 2004), the seasonal climatological seascape boundaries demarcate distinct nutrient ratios and NPP (this study).

Differences in environmental forcing across seascapes represent ecosystem-level variation in the processes that drive pCO_2. In particular, across the transition, summer production may not merely keep pace with, but rather exceed, the effect of warming in the summer (Takahashi et al., 2002, 2009). Some neural network –based predictions have resulted in regional biases in the seasonal cycle of pCO_2 (Telszewski et al., 2009, Landschützer et al., 2013), which may lead to inaccurate partitioning of drivers. However, in our study, the seasonality of predicted pCO_2 did not exhibit coherent zonal or meridional biases nor was there apparent seasonality within the Su-TRAN seascape. Furthermore, cruise-based studies in the NE Pacific (Lockwood et al., 2012; Howard et al., 2010; Juranek et al., 2012) support the our assertion that biological production drives pCO_2 patterns across the Su-TRAN seascape.

Conclusion:

The seascape framework described here considers dynamics in space and time simultaneously, including both advective and local shifts in state space, extending the landscape concept which has tended to focus on aggregates in space (O'Neill et al., 1992; Wu, 1999; but see Gillson, 2009). Dynamic, satellite-derived seascapes describe variability in biogeochemical patterns, NPP and environmental forcing of pCO_2. Seascapes can serve as indicators of spatiotemporal modifications in ecosystem structure and function (this study; Platt and Sathyendranath, 2008) and objective extents by which to extrapolate and/or compare *in situ* observations. We recognize that classification algorithms that use different sensors, attributes, assumptions of linearity, or dispersed organizational structure will result in different division of state space and thus, the spatiotemporal location of seascapes and their boundaries. However, we can learn much about the organization of the system by systematic comparison of method, attribute inclusion, and scale. In addition to the biogeochemical applications presented here, imposing objectively defined boundaries may be a means for applying the ecosystem concept to the open ocean (Cole, 2005; Kavanaugh et al., 2013). We are currently exploring the relevance of satellite seascapes to describe microbial communities, document boundary shifts associated with interannual forcing such as ENSO (e.g. Irwin and Oliver, 2009) and characterize long term seascape shifts apparent in marine ecosystem models, extending univariate understanding (e.g. Polovina et al., 2011) to a more multivariate ecosystem response. With increased technological capacity to sense both remotely and autonomously the aquatic environment, we now have the capacity for synoptic observations and characterization of unique combinations of physicochemical forcing and biological responses and/or feedbacks at several scales. Continued development of the seascape framework will help identify the major drivers of spatiotemporal variability of aquatic systems, and conversely, characterize the role that spatiotemporal variability plays in pelagic ecosystem functioning.

Figure captions:

Figure 1. Mean annual meridional surface velocities of the North Pacific (1998-2010). Current velocities are modeled from satellite altimetry (Ocean Surface Current model, OSCAR; Bonjean F. and G.S.E. Lagerloef, 2002). Overlain are general locations of major currents (white lines, italics), classic static province divisions (black lines; Longhurst 1997, 2008) and seasonal range of the transition zone chlorophyll front, TZCF (grey dashed, Polovina and others, 2001). See text for further description of natural features (Introduction 2.2) and comparisons between Longhurst provinces (Methods 3.6) and dynamic seascapes (this study).

Figure 2. Hierarchical structure of North Pacific Seascapes as defined by classification of satellite-derived SST, PAR, and chl-a. A. Percent aggregation defines emergent hierarchical levels marked by dashed lines in all subplots at N=3, 8, and 14 Seascapes. B. Relative Euclidean distances of seascapes at three hierarchical levels. Color-coding corresponds to Figures 3 and 4 (3rd level not colored). C. Percent of variance of SST, PAR, and chl-a explained through analysis of variance of seascapes at different hierarchical levels. Seascape identifiers and their abbreviations used in text and Table 1 are as follows: 1) Summer subtropical (Su-ST); 2) Winter subtropical (W-ST); 3) Oligotrophic boundary (OB); 4) Winter Transition (W-Tr); 5) Summer Transition (Su-Tr); 6) Mesotrophic boundary (MB); 7) Winter in subarctic (W-SA) 8) Summer subarctic (Su-SA).

Figure 3. Seasonal migration of seascapes in the North Pacific basin: Level 1. Eight seascapes were classified using a combination of a probabilistic self –organizing map and hierarchical clustering algorithm (PrSOM and HAC, respectively). Color codes indicate unique classifications and reflect relative concentrations of chl-a with red denoting higher concentrations and blue denoting lower concentrations.

Figure 4. Seasonal migration of seascapes in the North Pacific basin: Level 2. Eight seascapes were classified using a combination of PrSOM and HAC; color codes reflect different unique seascapes ranked by their relative concentrations of chl-a. White areas denote regions excluded because of cloud cover, ice, or high chl-a mask. Seascape identifiers and their abbreviations are as in Figure 2.

Figure 5. Seasonal migration of seascapes in the North Pacific basin: Level 3. Fourteen seascapes were classified using a combination of PrSOM and HAC; color codes reflect different seascapes ranked by their relative concentrations of chl-a.

Figure 6. Sensitivity of seascape boundaries to interannual changes in chl-a. The areal extent of Level 2 (N=8) seascapes are shown for the seasonal cycle. Open circles denote shifts in areal extent within seascapes for individual years. Solid circles denote shifts within climatological seascapes. Seascape identifiers are as follows: a) Summer subtropical (Su-ST); b) Winter subtropical (W-ST); c) Oligotrophic boundary (OB); d) Winter Transition (W-Tr); e) Summer Transition (Su-Tr); f) Mesotrophic boundary (MB); 7) Winter in subarctic (W-SA) g) Summer subarctic (Su-SA).

Figure 7. Effect sizes on pCO_2 of SST, salinity, season, and [chl-a]. Effect sizes were calculated using multiple linear regression analysis within seascapes (Methods: Section 3.6). Only the first two levels are presented, see Table 6 and Results (Section 4.3) for complete details.

711

Table 1. Summary Statistics of mean (standard error) satellite-derived SST, PAR, and chl-a within seascapes at three different hierarchical levels. % effective pixels depicts reduction in sample size following month-wise spatial decorrelation analysis. R^2 is proportion of variance explained by ANOVA of individual variables after decorrelation resampling (see methods for details). Seascapes that share letters are not statistically distinct from one another (Tukey-Kramer Honest Square Distance multiple comparisons analysis) in that variable.

	% effective pixel	SST	PAR	Log_{10} (chl-a)
Level 1: 3 seascapes				
Subtropics	0.18	24.3 (0.02)	46.4 (0.04)	-1.21 (0.001)
Transition	0.27	17.6 (0.02)	37.1 (0.05)	-0.71 (0.001)
Subarctic	0.47	8.3 (0.01)	25.0 (0.03)	-0.36 (0.001)
R^2		0.74	0.55	0.74
Level 2: 8 seascapes				
Summer Subtropics, Su-ST	0.24	27.6 (0.02)	52.3 (0.04)	-1.31 (0.001)
Winter Subtropics, W-ST	0.19	26.5 (0.02)	39.8 (0.04)	-1.27 (0.001)
Oligotrophic Boundary, OB	0.38	21.6 (0.02)	46.2 (0.03)	-1.13 (0.001)
Winter Transition, W-TR	0.28	22.3 (0.03)	26.8 (0.05)	-0.99 (0.002)
Summer Transition, Su-TR	0.44	16.0 (0.02)	40.7 (0.03)	-0.60 (0.001)
Mesotrophic Boundary, MB	0.15	12.8 (0.01)	25.5 (0.02)	-0.42 (0.001)
Winter Subarctic, W-SA	0.31	5.67 (0.01)	14.1 (0.03)	-0.40 (0.001)
Summer Subarctic, Su-SA	0.21	5.81 (0.01)	35.6 (0.03)	-0.26 (0.001)
R^2		0.89	0.86	0.80
Level 3: 14 Seascapes				
1	0.35	27.6 (0.02)	52.3 (0.03)	-1.31 (0.001)
2	0.43	26.5 (0.02)	39.8 (0.04)	-1.27 (0.001)
3	0.38	23.7 (0.02)	50.0 (0.04)	-1.16 (0.001)
4	0.19	20.3 (0.02)	44.1 (0.03)	-1.12 (0.001)
5	0.12	23.1 (0.02)	27.7 (0.05)	-1.06 (0.002)
6	0.15	19.4 (0.05)	23.6 (0.10)	-0.76 (0.004)a
7	0.24	20.2 (0.03)	36.7 (0.06)	-0.76 (0.002)a
8	0.05	14.8 (0.02)	17.1 (0.04)	-0.56 (0.001)
9	0.25	14.5 (0.02)	42.0 (0.03)	-0.55 (0.001)
10	0.15	3.43 (0.02)	13.8 (0.03)	-0.49 (0.001)
11	0.21	8.01 (0.02)	14.4 (0.03)	-0.31 (0.001)
12	0.40	12.1 (0.01)	28.3 (0.02)	-0.37 (0.001) b
13	0.14	8.29 (0.02)	37.2 (0.03)	-0.37(0.001) b
14	0.51	3.71(0.01)	34.2 (0.03)	-0.17(0.001)
R^2		0.94	0.90	0.83

Table 2. Nested analysis of variance: effect of hierarchical seascape level on nutrients, NPP and pCO_2. F-statistics for each explanatory variable are shown and are significant ($p<0.05$). R^2 denotes variance explained of fully nested model. Brackets denote the level of nesting with Level 3[Level 2, Level 1] describing variance explained by Level 3 seascapes after accounting for their nesting within Level 2 which is nested in Level 1.

	Salinity	NO_3	SiO_2	PO_4	NO_3 / SiO_2	NO_3 / PO_4	pCO_2	NPP
Level 1	1303	1074	772	1768	145	448	20	90
Level 2 [Level 1]	153	66	102	164	39	19	11	312
Level 3 [Level 2, Level1]	64	34	40	124	56	17	29	74
R^2	0.55	0.55	0.42	0.62	0.28	0.38	0.26	0.38

Table 3. Nested analysis of variance: relative role of among and within Level 2 seascape variability on nutrients, NPP, and pCO_2. F-statistics (proportion contributed) for each explanatory variable is shown. F-statistics are significant ($p<0.05$) unless otherwise noted. R^2 denotes variance explained of fully nested model. Brackets denote nesting within Level 2 seascapes.

	Salinity	NO_3	SiO_2	PO_4	NO_3 / SiO_2	NO_3 / PO_4	NPP	pCO_2
Level 2	168	174	74	166	53	102	17.6	15
Season[Level 2]	20	29	25	21	14	14	79.1	10
Space[Level 2]	18	5	15	13	5	^{NS} 1.8	4.9	5
Season*Space[Level2]	21	2.3	8	10	13	2.1	7.7	9
R^2	0.59	0.58	0.46	0.61	0.26	0.39	0.43	0.27

Table 4. Mean concentrations and ratios (+/- SE) of nutrients, pCO_2 and NPP in surface waters of Level 2 seascapes.

Seascape	N	NO_3 (µM)	SiO_2 (µM)	PO_4 (µM)	NO_3 / SiO_2	NO_3 /PO_4	pCO_2 (µatm)	NPP (mg C m^{-2} d^{-1})
Su-ST	385	0.26 (0.02)	2.51 (0.13)	0.08 (0.01)	0.13 (0.01)	4.04 (0.29)	360 (2)	416 (3)
W-ST	187	0.37 (0.09)	3.75 (0.31)	0.14 (0.01)	0.13 (0.03)	3.35 (0.52)	351 (3)	413 (4)
OB	700	0.25 0.02)	3.3 (0.09)	0.18 (0.01)	0.1 (0.01)	2.4 (0.17)	356 (2)	408 (3)
W-TR	282	0.61 (0.06)	2.89 (0.13)	0.15 (0.01)	0.23 (0.02)	5.25 (0.33)	331 (4)	359 (10)
Su-TR	953	1.67 (0.08)	5.1 (0.13)	0.36 (0.01)	0.3 (0.01)	4.53 (0.16)	338 (3)	600 (10)
MB	726	4.67 (0.17)	8.84 (0.25)	0.61 (0.01)	0.47 (0.01)	6.65 (0.18)	341 (2)	517 (8)
W-SA	233	6.31 (0.33)	11.8 (0.55)	0.85 (0.02)	0.57 (0.02)	6.96 (0.25)	347 (3)	266 (13)
Su-SA	519	7.53 (0.21)	14.0 (0.34)	0.9 (0.02)	0.59 (0.02)	7.8 (0.17)	343 (2)	660 (12)

Table 5. Comparison of classification efficiency between PRSOM seascapes and Longhurst provinces within and across months. Shown are F-statistics resulting from analyses of variance of surface [chl], NPP and a representative nutrient (PO4). All F-statistics are statistically significant ($p<0.05$) unless otherwise marked (NS). Bold= largest F-statistic and thus largest ratio of between group (explained) to within group (unexplained) variance. NPP and chl-a have been log10-transformed prior to analysis. Both weighted (W) and simple (S) means F-statistics across months are reported. T-ratio and p-value reflect 1-sided t-test (PrSOM-Longhurst).

	SeaWiFs [chl-a]			NPP (CbPM)			WOD- [Phosphate] (0-30 m)		
MO	N	PRSOM	LONG-HURST	N	PRSOM	LONG-HURST	N	PRSOM	LONG-HURST
1	150	**96.9**	42.1	150	**37.9**	30.6	139	**85.4**	45.8
2	153	**65.6**	32.7	153	9.8	**24.5**	150	34.2	**50.3**
3	172	**80.5**	31.4	172	16.8	**36.9**	166	**48.1**	40.3
4	335	**266**	86.9	335	5.0	**7.8**	302	**81.9**	28.4
5	475	**455**	90.8	475	**60.8**	17.9	458	**173**	86.9
6	489	**649**	276	489	**85.4**	34.2	444	**357**	196
7	514	**645**	347	514	**64.0**	45.2	493	**198**	112
8	568	**724**	326	568	**102**	62.0	538	**213**	194
9	296	**216**	151	296	**38.0**	32.2	245	49.5	**89.7**
10	273	**236**	118	273	**11.1**	5.5	242	**76.0**	44.5
11	197	**86.9**	38.4	197	**44.0**	33.4	168	**63.6**	57.1
12	94	**27.8**	26.9	94	**12.7**	2.1 NS	92	**35.7**	16.1
Mean (W)		**431**	187		**53.7**	32		**161**	106
Mean (S)		**296**	131		**40.6**	27.7		**117**	80.1
t-ratio		**3.79**			**2.02**			**2.45**	
p>t		**0.002**			**0.04**			**0.02**	

Table 6. Variable forcing of pCO2 by salinity, SST, [chl a] and Season within seascapes at different hierarchical levels. Effect sizes (+/-SE) for each explanatory variable are shown (Methods: Section 3.6). Effects are significant ($p<0.05$) unless otherwise noted (NS=not significant). R^2 denotes variance explained of full model. Pixels that were present in two or more seascapes were excluded. [chl-a] values were $\log_{10}$-transformed prior to analysis.

		N	mean(pCO2)	Salinity	SST	[chl a]	Season	R^2
1st level	Subtropics	749	353 (0.49)	-17.8 (1.7)	4.8 (1.4)	-7.6 (2.0)	10.1 (0.9)	0.26
	Transition	219	336 (0.8)	-32.6 (2.8)	*2.7 (3.0) NS*	-40 (2.4)	8.3 (2.0)	0.62
	Subarctic	703	346	129 (4.6)	-43.8 (1.7)	-24 (3.1)	*2.4 (1.8) NS*	0.67
2nd level	Su-ST	244	358 (0.6)	9.9(2.1)	15(1.5)	4.6 (2.1)	3.8 (1.2)	0.34
	W-ST	197	349 (0.7)	2.5 (2.5) NS	8.3(2.2)	5.2(2.5)	13 (8.7)	0.35
	OB	308	353 (0.8)	-33.9 (2.7)	11.3 (2.43)	-23.5 (3.0)	10.9 (1.6)	0.41
	W-TR	145	336 (0.9)	-15.2 (2.8)	-4.8 (2.6)	-29 (1.9)	4.5 (1.5)	0.64
	Su-TR	74	335 (1.54)	-29.4 (5.0)	10.9 (5.7)	-28.9 (3.0)	2.3 (5.0) NS	0.65
	MB	181	333 (0.8)	-18 (2.0)	3.4 (2.3) NS	-29 (3.6)	13.1 (2.1)	0.54
	W-SA	300	356 (0.9)	148 (7.0)	-39.3 (1.7)	-3.1 (3.5) NS	2.5 (1.3) NS	0.78
	Su-SA	222	342 (1.3)	125 (5.2)	-28.0 (4.0)	-22.5 (3.7)	-8.5 (3.8)	0.78
3rd level	SS1	244	358 (0.6)	9.9(2.1)	15(1.5)	4.6 (2.1)	3.8 (1.2)	0.34
	SS2	197	349 (0.7)	*2.5 (2.5) NS*	8.3(2.2)	5.2(2.5)	13 (8.7)	0.35
	SS3	107	352(1.35)	-12.3(4.5)	10.7(3.5)	-17.5 (5.2)	12.7 (2.8)	0.22
	SS4	102	359 (1.1)	-29 (3.3)	27 (3.3)	7.9 (3.2)	16.5 (2.3)	0.65
	SS5	41	338 (1.4)	*4.0(3.6) NS*	*2.5 (4.3) NS*	-11.4 (4.0)	6.4 (2.6)	0.44
	SS6	23	340 (1.4)	-10.6 (2.8)	8.8 (3.9)	-26.4 (2.5)	*3.0 (2.5) NS*	0.88
	SS7	9	343 (2.1)	*-4.4 (8) NS*	163 (43)	-180 (47)	84 (28)	0.84
	SS8	67	328 (0.9)	-14 (1.7)	*-2.5 (2.6) NS*	-15.2 (2.6)	9.0 (2.4)	0.68
	SS9	36	336 (2.2)	-23.2 (4.5)	*8.1 (6.1) NS*	-16.2 (4.2)	3.4 (3.5)	0.56
	SS10	114	377 (1.5)	18.2 (4.9)	-28.8 (3.8)	*-1.3 (7.9) NS*	*1.9 (2.4) NS*	0.51
	SS11	67	341 (1.7)	77.9 (8.7)	*0.1 (5.9) NS*	-13.7 (3.1)	*5.1 (5.1) NS*	0.73
	SS12	96	336 (1.1)	135 (6.7)	-17.8 (3.9)	*-4.4 (3.2) NS*	*2.9 (4.4) NS*	0.84
	SS13	107	337 (1)	-16.6 (3.6)	*3.9 (2.9) NS*	-25 (4.5)	6.0 (2.2)	0.38
	SS14	108	349 (1.8)	134 (7.6)	*34.2(5.8) NS*	-18 (5.1)	-17 (5.3)	0.82

Literature cited:

Anouar, F., F. Badran, and S. Thiria. 1998. Probabilistic self-organizing map and radial basis function networks. *Neurocomputing* **20**: 83–96

Belgrano, A., M. Lima, and N. C. Stenseth. 2004.Non-linear dynamics in marine-phytoplankton population systems : Emergent properties of complex marine systems: a macroecological perspective. *Marine Ecology Progress Series* **273**: 281–289.

Beaugrand, G., P. C. Reid, and F. Ibañez. 2000. Biodiversity of North Atlantic and North Sea calanoid copepods . *Marine Ecology Progress Series* **204**: 299–303.

Bograd, S. J., D. G. Foley, F. B. Schwing, C. Wilson, R. M. Laurs, J. J. Polovina, E. A. Howell, and R. E. Brainard (2004), On the seasonal and interannual migrations of the transition zone chlorophyll front, *Geophys. Res. Lett.*, 31, L17204, doi:10.1029/2004GL020637.

Cole, J. J. Communication between terrestrial and marine ecologists : loud, sometimes abrasive, but healthy and occasionally useful : Bridging the gap between aquatic and terrestrial ecology. *Marine Ecology Progress Series* **304**: 272–274.

Deutsch, C., N. Gruber, R. M. Key, J. L. Sarmiento, and A. Ganachaud. 2001.Denitrification and N2 fixation in the Pacific Ocean. *Global Biogeochemical Cycles* **15**: 483–506.

Devred, E., Sathyendranath, S., Platt, T., 2007. Delineation of ecological provinces using ocean colour radiometry. *Marine Ecology Progress Series* 346, 1-13.

Devred, E., Sathyendranath, S., Platt, T., 2009. Decadal changes in ecological provinces of the Northwest Atlantic Ocean revealed by satellite observations. *Geophysical Research Letters* 36, L19607, doi:10.1029/2009GL039896

Doney, S. C., M. Ruckelshaus, J. Emmett Duffy, J. P. Barry, F. Chan, C. A. English, H. M. Galindo, J. M. Grebmeier, A. B. Hollowed, N. Knowlton, J. Polovina, N. N. Rabalais, W. J. Sydeman, and L. D. Talley. 2012. Climate Change Impacts on Marine Ecosystems. *Annual Review of Marine Science* **4**: 11–37

Dutkiewicz, S., B.A. Ward, F. Monteiro, And M.J. Follows, 2012: Interconnection between nitrogen fixers and iron in the Pacfic Ocean: Theory and numerical model. *Global Biogeochemical Cycles* , 26, GB1012, doi:10.1029/2011GB004039

Evans, W., P. G. Strutton, and F. P. Chavez. 2009. Impact of tropical instability waves on nutrient and chlorophyll distributions in the equatorial Pacific. *Deep Sea Research Part I: Oceanographic Research Papers* **56**: 178–188

Fortin, M.-J., and M. R. T. Dale. 2005. *Spatial Analysis: A Guide for Ecologists*, Cambridge University Press.

Friedrich, T., and A. Oschlies. 2009. Neural network-based estimates of North Atlantic surface pCO 2 from satellite data: A methodological study. *Journal of Geophysical Research* **114**: C03020

Gillson, L. 2009. Landscapes in Time and Space. *Landscape Ecology*, **24**(2), 149–155.

Gruber, 2011 Warming up, turning sour, losing breath: Ocean biogeochemistry under global change, *Phil. Trans. R. Soc. A*, **369**, 1980-1996, doi:10.1098/rsta.2011.0003

Hales, B., P. G. Strutton, M. Saraceno, R. Letelier, T. Takahashi, R. Feely, C. Sabine, and F. Chavez. 2012. Satellite-based prediction of pCO_2 in coastal waters of the eastern North Pacific. *Progress in Oceanography,* **103**: 1-15

Hardman-Mountford, N. J., T. Hirata, K. A. Richardson, and J. Aiken. 2008. An objective methodology for the classification of ecological pattern into biomes and provinces for the pelagic ocean. *Remote Sensing of Environment* **112**: 3341–3352.

Hsieh, C., S. M. Glaser, A. J. Lucas, and G. Sugihara. 2005. Distinguishing random environmental fluctuations from ecological catastrophes for the North Pacific Ocean. *Nature* **435**: 336–340.

Irwin, A. J., and Oliver, M. J. 2009. Are ocean deserts getting larger ?, *Geophysical Research Letters* **36**: 1–5. doi:10.1029/2009GL039883

Jain, A. K., R. C. Dubes, and C. C. Chen. 1987. Bootstrap techniques for error estimation. I*EEE Transactions on Pattern Analysis and Machine Intelligence* **9**: 628–633

Jassby, A. D., and T. Platt. 1976. Mathematical Formulation of the Relationship Between Photosynthesis and Light for Phytoplankton. L*imnology and Oceanography* **21**: 540–547.

Kavanaugh, M.T., G.W. Holtgrieve, H. Baulch, J. R. Brum, M. L. Cuvelier, C. T. Filstrup, K. J. Nickols, G.E. Small. 2013. A salty divide in ASLO? *Limnology and Oceanography Bulletin* **22 (2):** 34-37

Karl, D. M., M. J. Church, J. E. Dore, R. M. Letelier, and C. Mahaffey. 2012. Predictable and efficient carbon sequestration in the North Pacific Ocean supported by symbiotic nitrogen fixation. *Proceedings of the National Academy of Sciences of the United States of America* **109**: 1842–9

Karl, D. M. and R. M. Letelier. 2009. Seascape microbial ecology: Habitat structure, biodiversity and ecosystem function. In: S. A. Levin (Ed.), *Guide to Ecology*, Princeton University Press, Princeton, New Jersey, pp. 488–500

Kotliar, N. B., and J. A. Wiens. 1990. Multiple Scales of Patchiness and Patch Structure: A Hierarchical Framework for the Study of Heterogeneity. *Oikos* **59**: 253–260.

Lachkar, Z., and N. Gruber. 2012. A comparative study of biological production in eastern boundary upwelling systems using an artificial neural network. *Biogeosciences* **9**: 293–308

Landschützer, P., Gruber, N., Bakker, D. C. E., Schuster, U., Nakaoka, S., Payne, M. R., Sasse, T., and Zeng, J.2013. A neural network-based estimate of the seasonal to inter-annual variability of the Atlantic Ocean carbon sink. *Biogeosciences Discuss*., **10**, 8799-8849, doi:10.5194/bgd-10-8799-2013, 2013

Letelier, R.M., R.R. Bidigare, D.V. Hebel, M. Ondrusek, C.D. Winn, D.M. Karl . 1993. Temporal variability of phytoplankton community structure based on pigment analysis. *Limnol. Oceanogr*., **38**, 1420-1437

Levin, S. A. 1976. Population dynamic models in heterogeneous environments. *Annual Review of Ecology and Systematics* **7**: 287–310

Levin, S. A., and M. Whitfield. 1994. Patchiness in Marine and Terrestrial Systems: From Individuals to Populations [and Discussion]. *Philosophical Transactions of the Royal Society B: Biological Sciences* **343**: 99–103

Litzow, M. A., and L. Ciannelli. 2007. Oscillating trophic control induces community reorganization in a marine ecosystem. *Ecology Letters* **10**: 1124–1134

Longhurst, A. R. 1998 (1st edition) and 2007 (2nd edition) . Ecological Geography of the Sea. Elsevier Press. London UK

Lockwood D, Quay, P.D., Kavanaugh, M.T, Juranek, LW, Feely, R. 2012. Influence of net community production on air-sea CO2 flux in the Northeast Pacific. *Global Biogeochemical Cycles* **26**: GB4010. doi:10.1029/2012GB004380.

Lubchenco, J., and L. E. Petes. 2010. The Interconnected Biosphere: Science at the Ocean's Tipping Points. *Oceanography* **23**: 115–129

Luo, Y.-W., S.C. Doney, L.A. Anderson, M. Benavides, I. Berman-Frank, A. Bode, S. Bonnet, K.H. Boström, D. Böttjer, D.G. Capone, E.J. Carpenter, Y.L. Chen, M.J. Church, J.E. Dore, L.I. Falcón, A. Fernández, R.A. Foster, K. Furuya, F. Gómez, K. Gundersen, A.M. Hynes, D.M. Karl, S. Kitajima, R.J. Langlois, J. LaRoche, R.M. Letelier, E. Marañón, D.J. McGillicuddy Jr., P.H. Moisander, C.M. Moore, B. Mouriño-Carballido, M.R. Mulholland, J.A. Needoba, K.M. Orcutt, A.J. Poulton, E. Rahav, P. Raimbault, A.P. Rees, L. Riemann, T. Shiozaki, A. Subramaniam, T. Tyrrell, K.A. Turk-Kubo, M. Varela, T.A. Villareal, E.A. Webb, A.E. White, J. Wu, and J.P. Zehr, 2012: Database for diazotrophs in global ocean: abundances, biomass and nitrogen fixation rates, *Earth Syst. Sci. Data*, **4,** 47-73, doi:10.5194/essd-4-47-2012

Luo, Y.-W., I.D. Lima, D.M. Karl, and S.C. Doney, Data-based assessment of environmental controls on global marine nitrogen fixation, *Biogeosciences*, submitted. (*Biogeosciences Discuss*., 10, 7367-7412, 2013)

McCune, B., Grace, J. B., & Urban, D. L. (2002). *Analysis of ecological communities* (Vol. 28). Gleneden Beach, Oregon: MjM Software Design

Mitchell JG, Yamazaki H, Seuront L, Wolk F & Hua L (2008) Phytoplankton patch patterns: seascape anatomy in a turbulent ocean. *Journal of Marine Systems*, 69, 247-253.

Murawski, S. A., J. H. Steele, P. Taylor, M. J. Fogarty, M. P. Sissenwine, M. Ford, and C. Suchman. 2010. Why compare marine ecosystems? *ICES Journal of Marine Science* **67**: 1–9

Oliver, M. J., and A. J. Irwin. 2008. Objective global ocean biogeographic provinces. *Geophysical Research Letters* **35** 15 (2008): L15601.

O'Neill, R. V., R. H. Gardner, and M. G. Turner. 1992. A hierarchical neutral model for landscape analysis. *Landscape Ecology* 7: 55–61

Park, G.-H., R. Wannikhof, S. C. Doney, T. Takahashi, K. Lee, R. A. Feely, C. L. Sabine, J. Trinanes, and I. D. Lima. 2010. Variability of global net sea-air CO2 fluxes over the last three decades using empirical relationships. *Tellus* B **62**: 352–368

Platt, T., and S. Sathyendranath. 1999. Spatial structure of pelagic ecosystem processes in the global ocean. *Ecosystems* **2**: 384–394 .

Platt, T., and S. Sathyendranath. 2008. Ecological indicators for the pelagic zone of the ocean from remote sensing. *Remote Sensing of Environment* **112**: 3426–3436

Polovina, J. J., E. Howell, D. R. Kobayashi, and M. P. Seki. 2001. The transition zone chlorophyll front, a dynamic global feature defining migration and forage habitat for marine resources. *Progress in Oceanography* **49**: 469–483

Polovina, J. J., J. P. Dunne, P. A. Woodworth, and E. A. Howell. 2011. Projected expansion of the subtropical biome and contraction of the temperate and equatorial upwelling biomes in the North Pacific under global warming. *ICES Journal of Marine Science: Journal du Conseil* **68**.6: 986-995

Richardson, A., C. Risien, and F. Shillington. 2003. Using self-organizing maps to identify patterns in satellite imagery. *Progress in Oceanography* **59**: 223–239

Saraceno, M., C. Provost, and M. Lebbah. 2006. Biophysical regions identification using an artificial neuronal network: A case study in the South Western Atlantic. *Advances in Space Research.* **37**: 793–805

Siegel, D. A., T. K. Westberry, M. C. O'Brien, N. B. Nelson, A. F. Michaels, J. R. Morrison, A. Scott, E. A. Caporelli, J. C. Sorensen, S. Maritorena, S. A. Garver, E. A. Brody, J. Ubante, and M. A. Hammer. 2001. Bio-optical modeling of primary production on regional scales:

the Bermuda BioOptics project. *Deep-Sea Research Part IIi-Topical Studies in Oceanography* **48**: 1865–1896

Siegel, D. A., Behrenfeld, M. J., Maritorena, S., McClain, C. R., Antoine, D., Bailey, S. W., Bontempi, P. S., et al. (2013). Regional to global assessments of phytoplankton dynamics from the SeaWiFS mission. *Remote Sensing of Environment*, 135(0), 77–91.

Somerville, M. 1853. Physical geography. Lea & Blanchard. Michigan Historical Reprint Series, University of Michigan, Ann Arbor, MI.

Steele, J. H. 1989. The ocean landscape? *Landscape Ecology* **3**: 185–192

Steele, J. H. 1991. Can ecological theory cross the land-sea boundary? *Journal of Theoretical Biology* **153**: 425–436

Steele, J. H., and E. W. Henderson. 1992. A simple model for plankton patchiness. *Journal of Plankton Research* **14**: 1397–1403

Takahashi, T., S. C. Sutherland, C. Sweeney, A. Poisson, N. Metzl, B. Tilbrook, N. Bates, R. Wanninkhof, R. A. Feely, C. Sabine, J. Olafsson, and Y. Nojiri. 2002. Global sea-air CO2 flux based on climatological surface ocean pCO(2), and seasonal biological and temperature effects. *Deep-Sea Research Part II-Topical Studies in Oceanography* **49**: 1601–1622

Takahashi, T., S. C. Sutherland, R. Wanninkhof, C. Sweeney, R. A. Feely, D. W. Chipman, B. Hales, G. Friederich, F. Chavez, C. Sabine, A. Watson, D. C. E. Bakker, U. Schuster, N. Metzl, H. Yoshikawa-Inoue, M. Ishii, T. Midorikawa, Y. Nojiri, A. Kortzinger, T. Steinhoff, M. Hoppema, J. Olafsson, T. S. Arnarson, B. Tilbrook, T. Johannessen, A. Olsen, R. Bellerby, C. S. Wong, B. Delille, N. R. Bates, and H. J. W. de Baar. 2009. Climatological mean and decadal change in surface ocean pCO(2), and net sea-air CO2 flux over the global oceans. *Deep-Sea Research Part II: Topical Studies in Oceanography* **56**: 554–577

Telszewski, M., Chazottes, A., Schuster, U., Watson, A. J., Moulin, C., Bakker, D. C. E., González-Dávila, M., Johannessen, T., Körtzinger, A., Lüger, H., Olsen, A., Omar, A., Padin, X. A., Ríos, A. F., Steinhoff, T., Santana-Casiano, M., Wallace, D. W. R., and Wanninkhof, R.2009. Estimating the monthly $p\mathrm{CO_2}$ distribution in the North Atlantic using a self-organizing neural network, *Biogeosciences*, 6, 1405-1421, doi:10.5194/bg-6-1405-2009, 2009

Turner, M. G. 2005. Landscape ecology: What is the state of the science? *Annual Review of Ecology Evolution and Systematics* **36**: 319–344

Turner, M. G., R. H. Gardner, and R. V. O'Neill. 2001. *Landscape Ecology in Theory and Practice: Pattern and Process* , Springer-Verlag, New York

Troll, C. 1950: Die geographische Landschaft und ihre Erforschung. Studium Generale 3(4/5):163–181 In: Wiens, J.A., Moss, M.R., Turner, M.G. & Mladenoff, D.J. (eds): *Foundation papers in landscape ecology*. New York, Columbia University Press

Venrick, E. L. 1974. The Distribution and Significance of Richelia intracellularis Schmidt in the North Pacific Central Gyre. *Limnology and Oceanography* **19**: 437–445.

Vichi, M., J. I. Allen, S. Masina, and N. J. Hardman-Mountford (2011), The emergence of ocean biogeochemical provinces: A quantitative assessment and a diagnostic for model evaluation, *Global Biogeochem. Cycles*, 25, GB2005, doi:10.1029/2010GB003867.

Villareal, T. A. 1991. Nitrogen-fixation by the cyanobacterial symbiont of the diatom genus Hemiaulus. *Marine Ecology Progress Series. 76*(2), 201-204.

Ward, J. H. 1963. Hierarchical Grouping to Optimize an Objective Function. *Journal of the American Statistical Association* **58**: 236–244

Weber, T. S., and C. Deutsch. 2010. Ocean nutrient ratios governed by plankton biogeography. *Nature* **467**: 550–4

Westberry TK, Behrenfeld MJ, Siegel DA, Boss E. 2008. Carbon-based primary productivity modeling with vertically resolved photoacclimation. *Global Biogeochem. Cycles* 22:GB2024

White, A. E., Y. H. Spitz, and R. M. Letelier. 2007. What factors are driving summer phytoplankton blooms in the North Pacific Subtropical Gyre? *Journal of Geophysical Research* **112**: 1–11

Winn, C.D., L. Campbell, J.R. Christian, R.M. Letelier, D.V. Hebel, J.E. Dore, L. Fujieki, and D.M. Karl. 1995. Seasonal variability in the phytoplankton community of the North Pacific Subtropical Gyre, *Global Biogeochem. Cycles*, **9**, 605-620

Wilson, C., T. A. Villareal, N. Maximenko, S. J. Bograd, J. P. Montoya, and C. A. Schoenbaechler. 2008. Biological and physical forcings of late summer chlorophyll blooms at 30°N in the oligotrophic Pacific. *Journal of Marine Systems* **69**: 164–176

Wu, J., and O. L. Loucks. 1995. From Balance of Nature to Hierarchical Patch Dynamics: A Paradigm Shift in Ecology. *The Quarterly Review of Biology* **70**: 439–466.

Wu, J. 1999 Hierarchy and scaling : Extrapolating information along a scaling ladder. Canadian *Journal of Remote Sensing*, 25(4), 367–380.

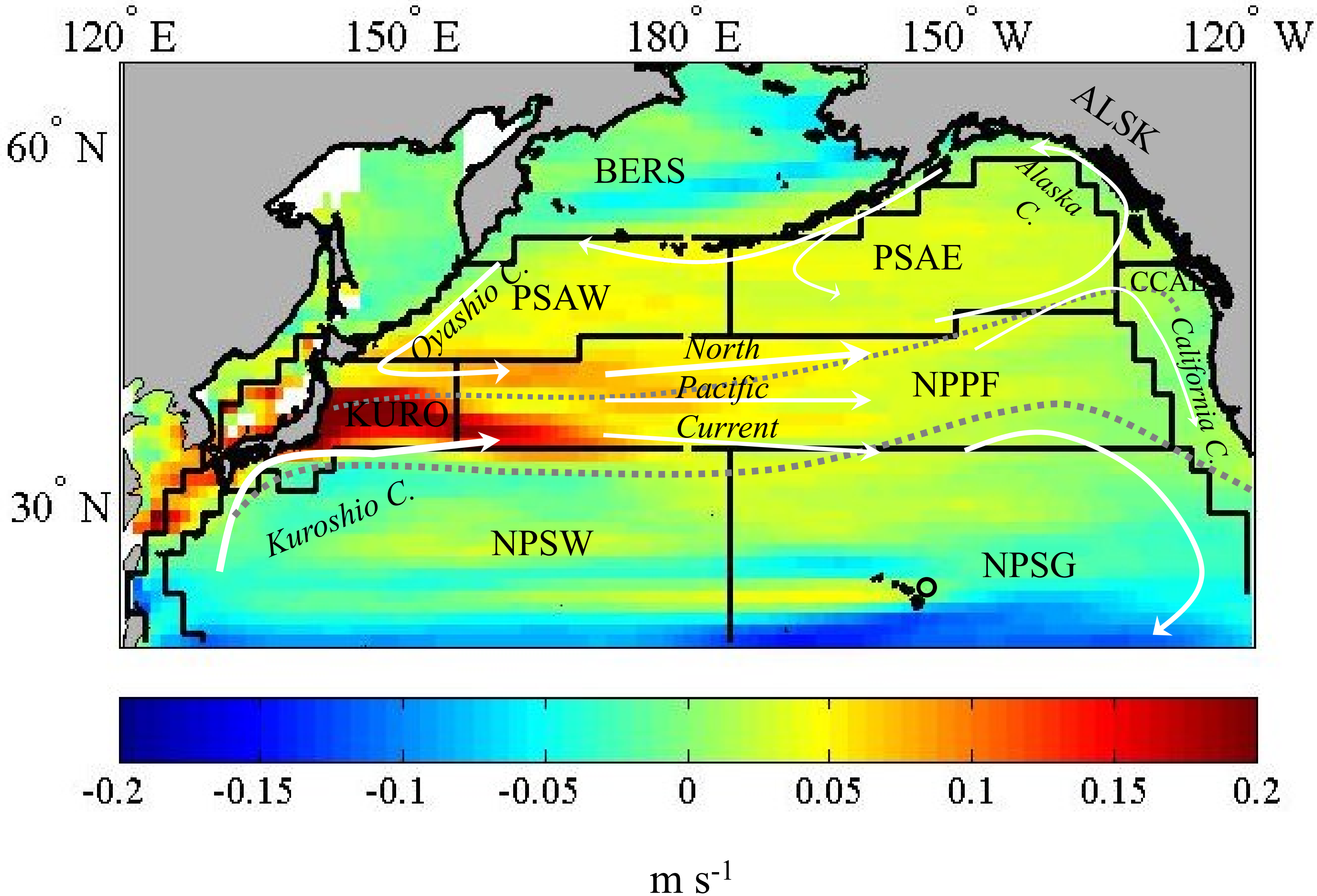
120° E
150° E
180° E
150° W
120° W
60° N
30° N
BERS
ALSK
PSAE
Alaska C.
CCAL
PSAW
Oyashio C.
North Pacific Current
NPPF
California C.
KURO
Kuroshio C.
NPSW
NPSG
-0.2
-0.15
-0.1
-0.05
0
0.05
0.1
0.15
0.2
m s-1

Figure 1

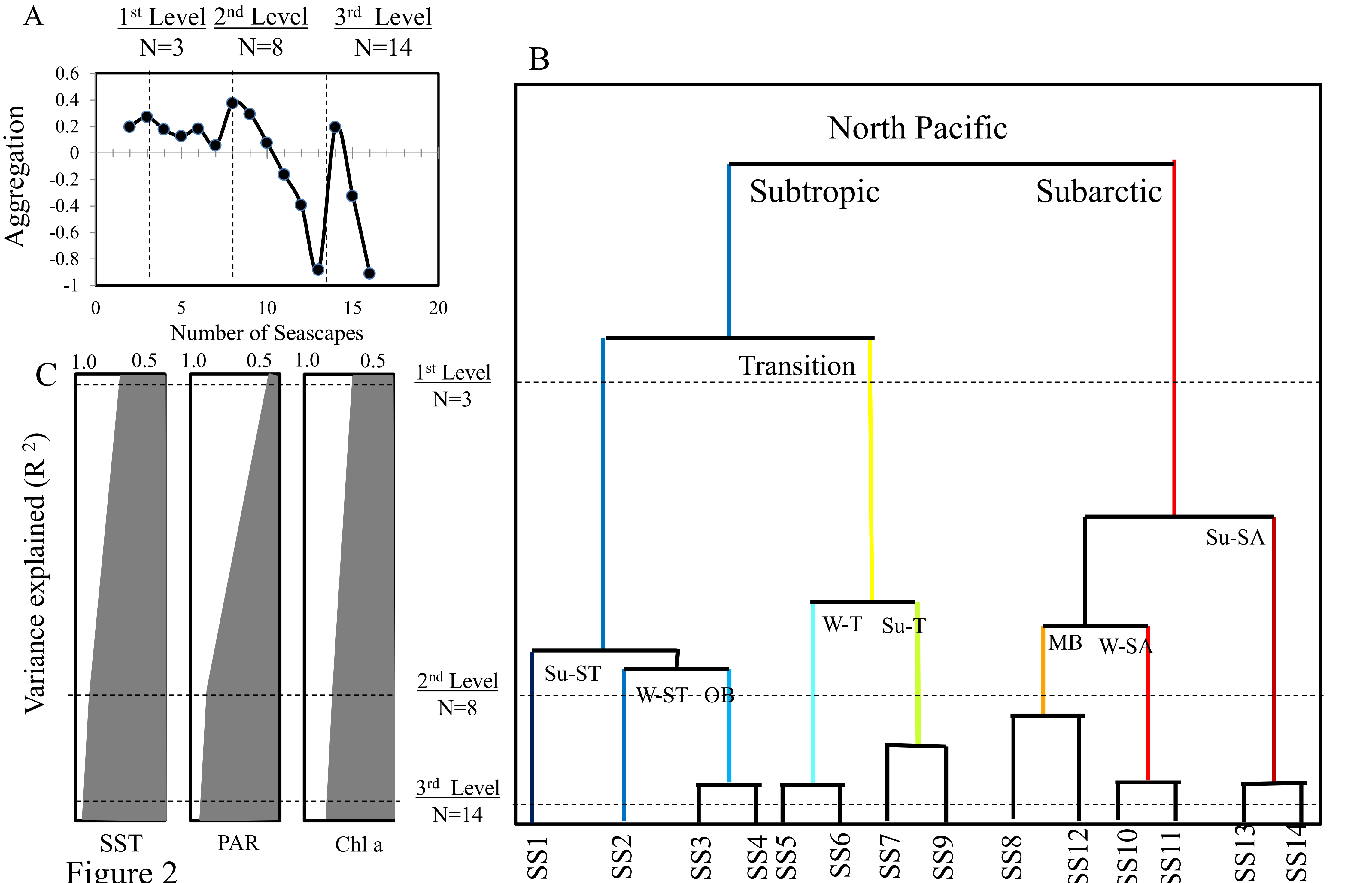

A
1st Level N=3
2nd Level N=8
3rd Level N=14
Aggregation
Number of Seascapes
B
North Pacific
Subtropic
Subarctic
Transition
Su-SA
W-T
Su-T
MB
W-SA
Su-ST
W-ST
OB
SS1
SS2
SS3
SS4
SS5
SS6
SS7
SS9
SS8
SS12
SS10
SS11
SS13
SS14
C
Variance explained (R 2)
SST
PAR
Chl a

Figure 2

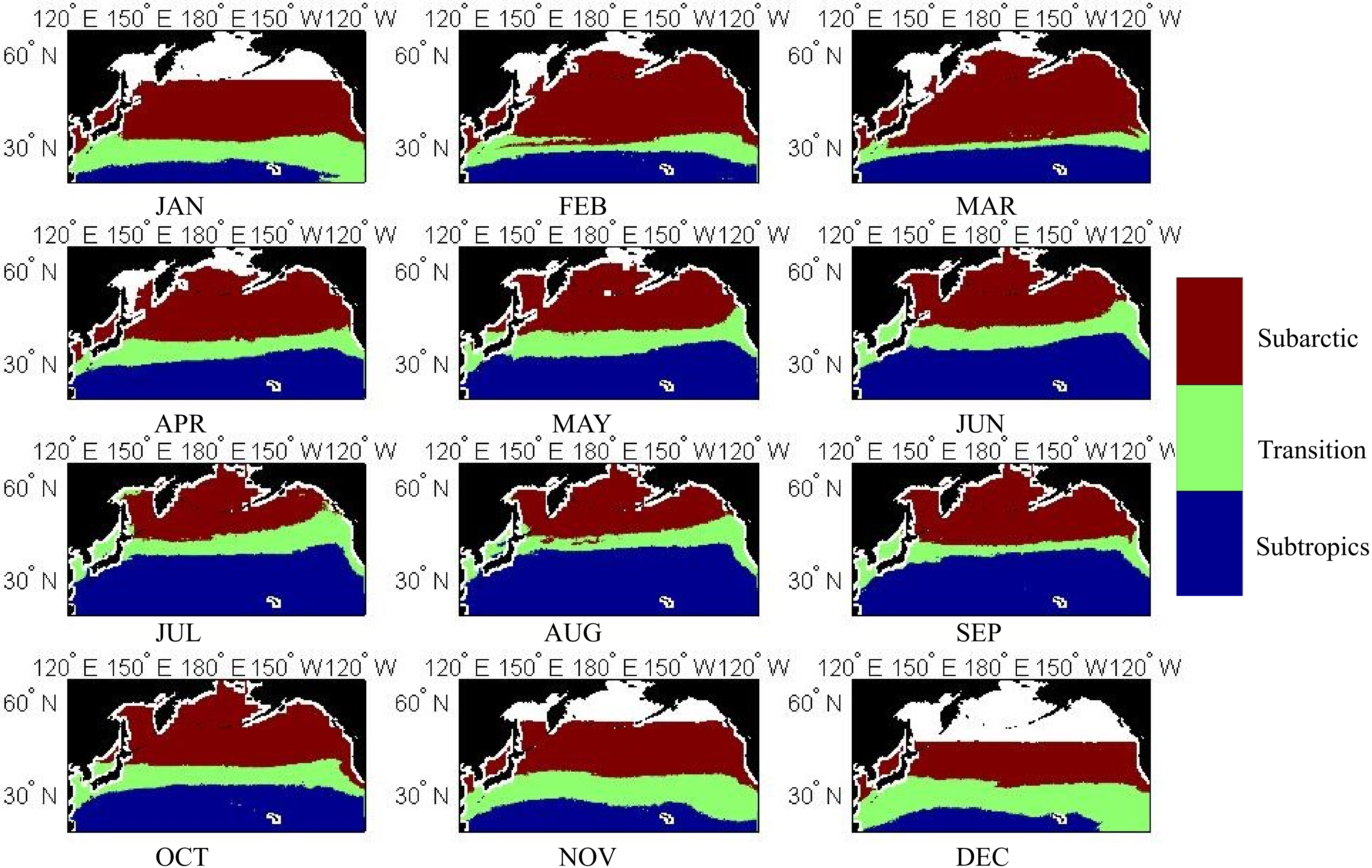
120° E 150° E 180° E 150° W 120° W
60° N
30° N
JAN
FEB
MAR
APR
MAY
JUN
JUL
AUG
SEP
OCT
NOV
DEC
Subarctic
Transition
Subtropics

Figure 3

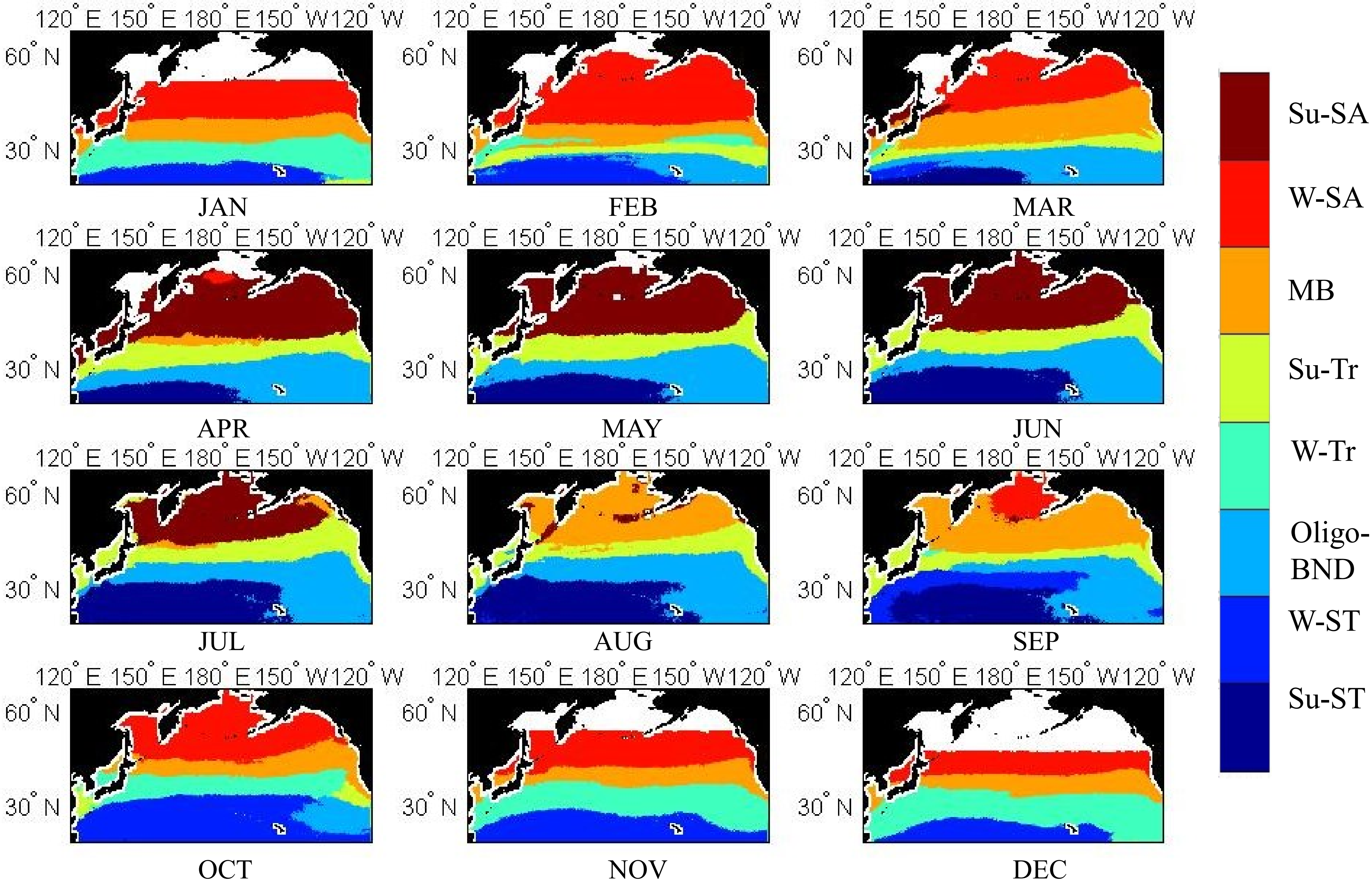
120° E 150° E 180° E 150° W 120° W
60° N
30° N
JAN
FEB
MAR
APR
MAY
JUN
JUL
AUG
SEP
OCT
NOV
DEC
Su-SA
W-SA
MB
Su-Tr
W-Tr
Oligo-BND
W-ST
Su-ST

Figure 4

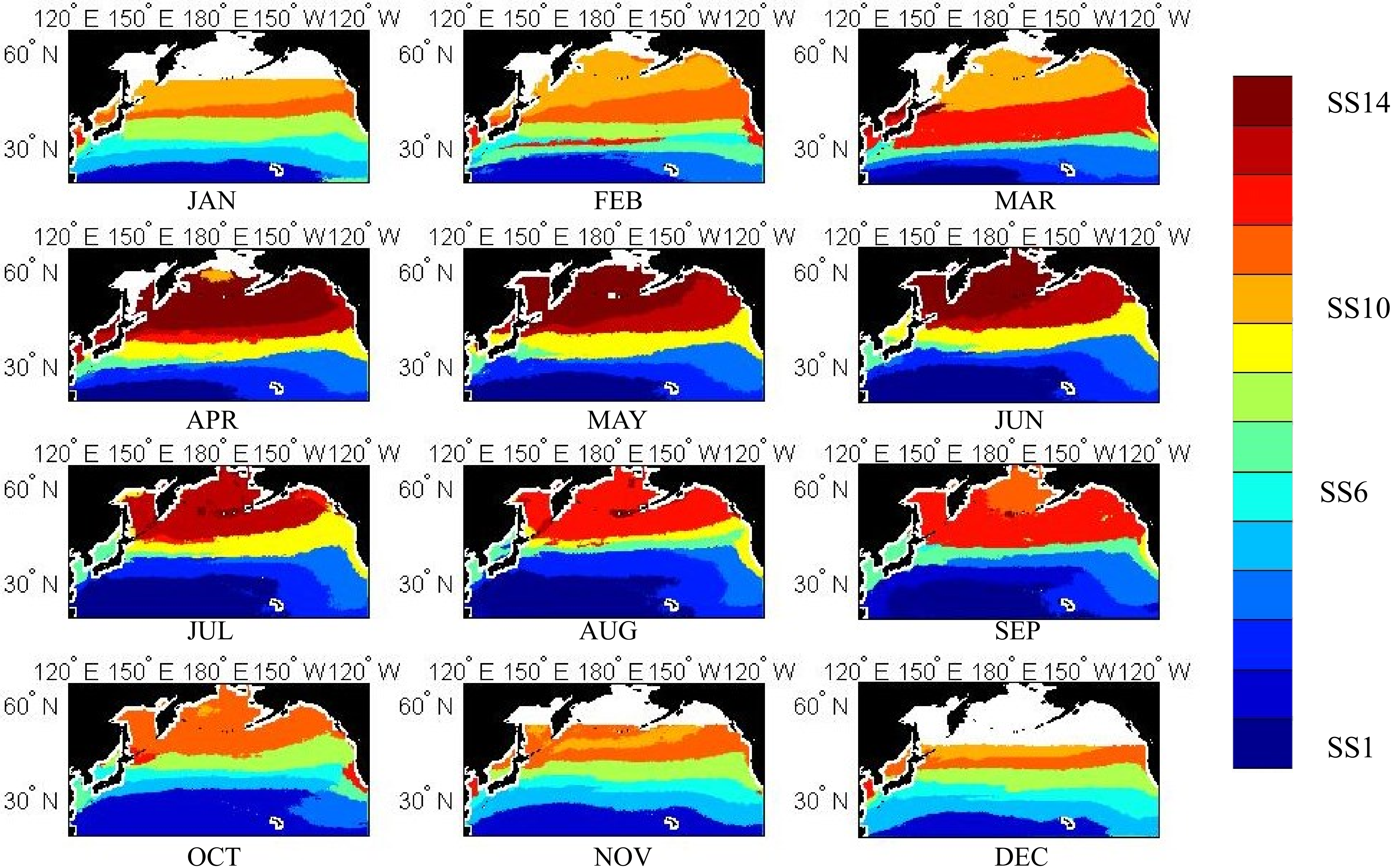
120° E 150° E 180° E 150° W 120° W
60° N
30° N
JAN
FEB
MAR
APR
MAY
JUN
JUL
AUG
SEP
OCT
NOV
DEC
SS14
SS10
SS6
SS1

Figure 5

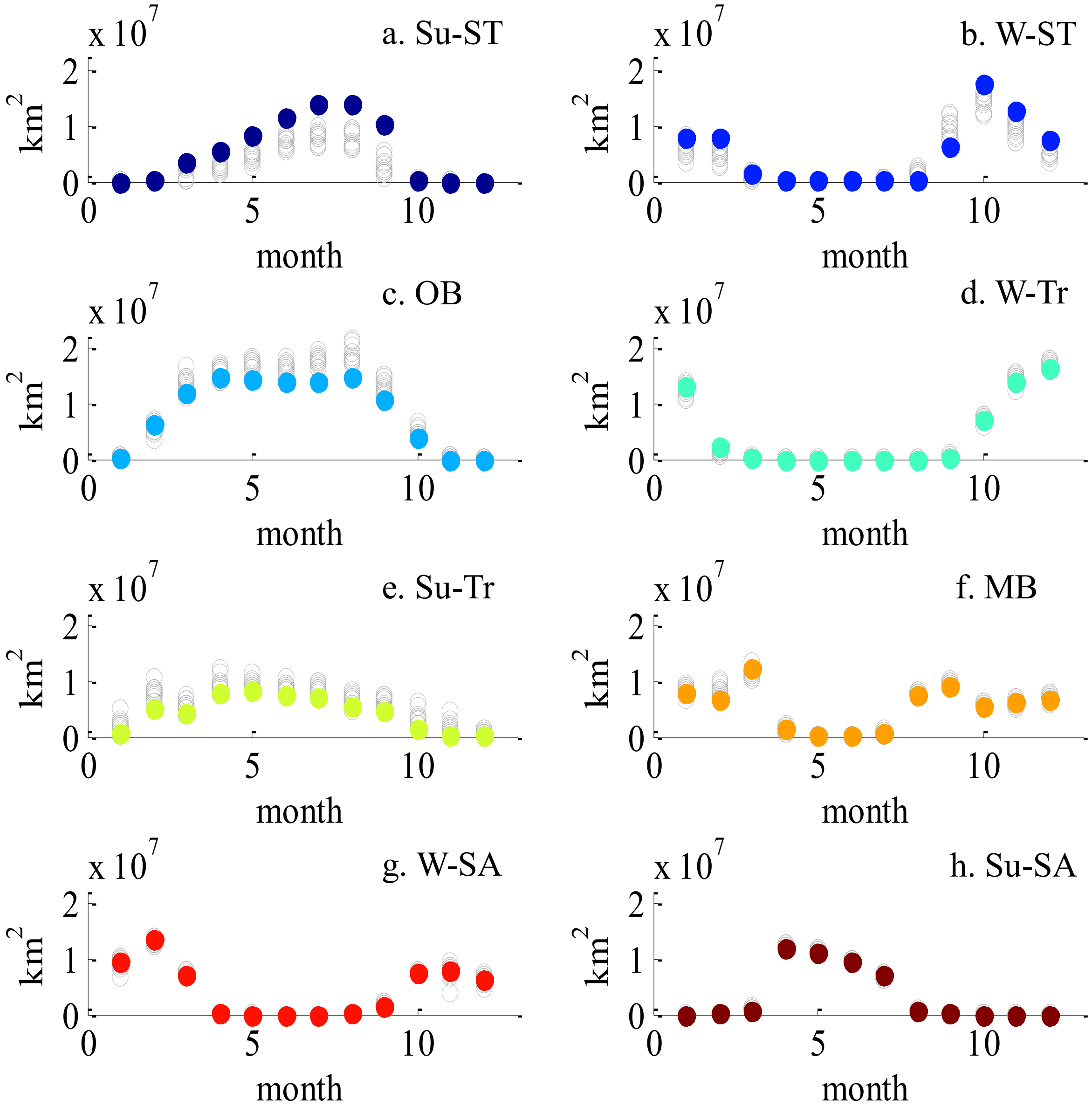

a. Su-ST
b. W-ST
c. OB
d. W-Tr
e. Su-Tr
f. MB
g. W-SA
h. Su-SA
x 10^7
km^2
month
0
1
2
0
5
10

Figure 6

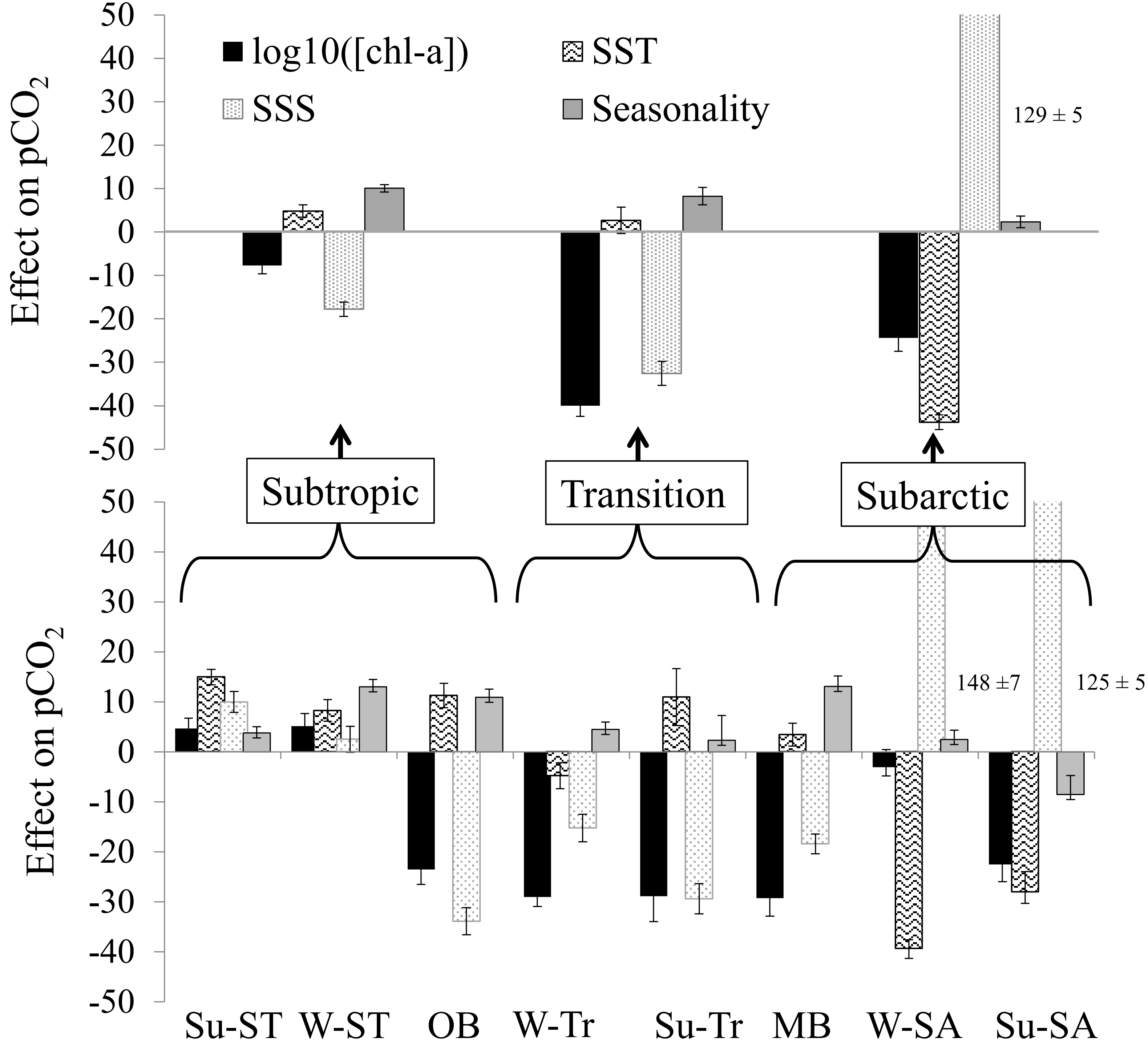

log10([chl-a])
SST
SSS
Seasonality
129 ± 5
Effect on pCO_2
Subtropic
Transition
Subarctic
148 ±7
125 ± 5
Su-ST
W-ST
OB
W-Tr
Su-Tr
MB
W-SA
Su-SA

Figure 7